Titre: Title:	Thermodynamic Evaluation and Optimization of the As–Cd, As–Zn and As–Cd–Zn Systems
Auteurs: Authors:	Oumaima Kidari, & Patrice Chartrand
Date:	2023
Type:	Article de revue / Article
Référence: Citation:	Kidari, O., & Chartrand, P. (2023). Thermodynamic Evaluation and Optimization of the As–Cd, As–Zn and As–Cd–Zn Systems. Metallurgical and Materials Transactions B, 2023(5), 2793-2814. https://doi.org/10.1007/s11663-023-02875-5

Document publié chez l'éditeur officiel
Document issued by the official publisher

Titre de la revue: Journal Title:	Metallurgical and Materials Transactions B (vol. 2023, no. 5)
Maison d'édition: Publisher:	Springer
URL officiel: Official URL:	https://doi.org/10.1007/s11663-023-02875-5
Mention légale: Legal notice:	

Thermodynamic Evaluation and Optimization of the As–Cd, As–Zn and As–Cd–Zn Systems

OUMAIMA KIDARI and PATRICE CHARTRAND

In this work, a critical evaluation of all available phase diagrams and thermodynamic data for the As–Cd, As–Zn and As–Cd–Zn systems has been performed and thermodynamic assessments over the whole composition ranges are presented using the CALPHAD method. To predict thermodynamic properties and phase equilibria for these systems, the Modified Quasichemical Model for short range ordering was used for the liquid phase and the Compound Energy Formalism was used for the solid solutions. The optimized binary systems are in good agreement with existing experimental data. Within the ternary system predicted phase equilibria, the $ZnAs_2-CdAs_2$ and $Zn_3As_2-Cd_3As_2$ sections are in good agreement with the experimental data. Also, the eutectic temperature is accurately optimized for $ZnAs_2-Cd_3As_2$ and $Zn_3As_2-CdAs_2$. However, the calculated liquidus of these two joins are less satisfactory compared to the experimental data. This is most likely due to the polymerization behavior of arsenic and its multivalence, which is not considered by the model used in this work.

I. INTRODUCTION

As ore concentrates available in the market contain increasing amounts of arsenic, their use will be unavoidable to ensure the viability of the smelting industry. The industry wishes to reduce the atmospheric emissions of this harmful impurity and thus comply with environmental standards. Just like arsenic, cadmium has toxic properties and its presence, particularly in copper smelters, has led to growing concerns of contamination in the surrounding areas due to its high mobility in the environment and its long body retention time.[1] Cadmium is usually associated with zinc sulfide present in complex ores.[2] To help find a solution to reduce toxic emissions caused by the treatment of copper concentrates in smelters, the development of thermodynamic models of compounds and mixtures, and their associated databases, for systems involving arsenic and other impurities is of much interest for the copper industry. In the present article, the available experimental data of the two binary systems As–Cd and As–Zn and the ternary system As–Cd–Zn is presented and critically evaluated. A set of model parameters is optimized for each phase to predict thermodynamic properties and phase equilibria for these systems. The Modified Quasichemical Model (MQM) in the Pair Approximation suggested by Pelton et al.[3,4] was used for the liquid phases, and the Compound Energy Formalism (CEF) suggested by Sundman and Ågren[5] was used for solid solutions. All calculations and optimizations in this work were performed with the FactSage™ thermochemical software.[6–8] The previous assessments of the As–Zn system by Dessureault[9] as well as the one by Ghasemi and Johansson[10] are presented and discussed briefly, similarly to the previous assessments of the Cd–Zn system by Zabdyr[11] and Min et al.[12] The parameters suggested by Zabdyr[11] are incorporated into the database and are used in this work to evaluate the ternary As–Cd–Zn.

II. LITERATURE REVIEW

A. As–Cd and As–Zn Binary Phase Diagrams

There are many similarities between the As–Cd and As–Zn systems. Each system includes two stable compounds at ambient pressure, Cd_3As_2 and Zn_3As_2 that undergo polymorphic transformations as well as $CdAs_2$ and $ZnAs_2$. The crystal structures of the solid phases are presented in Table I. The available standard enthalpies of formation of the intermediate compounds in both As–Cd and As–Zn systems are shown in Figure 1.

OUMAIMA KIDARI and PATRICE CHARTRAND are with the Chemical Engineering, Center for Research in Computational Thermochemistry (CRCT), Polytechnique Montréal, Box 6079, Station Downtown, Québec H3C 3A7, Canada. Contact e-mail: oumaima.kidari@polymtl.ca

Table I.   Crystallographic Description of the Phases in As–Cd and As–Zn Systems

Phase	Person Symbol	Space Group	Strukturbericht Designation	References
Cd_3As_2	cF12	$Fm\overline{3}m$	C1	[13]
				[14]
Zn_3As_2				
Cd_3As_2	tP40	$P4_2/nmc$	$D5_9$	[15]
Zn_3As_2				[13]
Cd_3As_2	tP160	$P4_2/nbc$	—	[13]
Cd_3As_2	tI160	$I4_1cd$	—	[16]
Zn_3As_2				[13]
$CdAs_2$	tI12	$I4_122$	—	[17]
$ZnAs_2$	mP24	$P2_1/c$	—	[18]
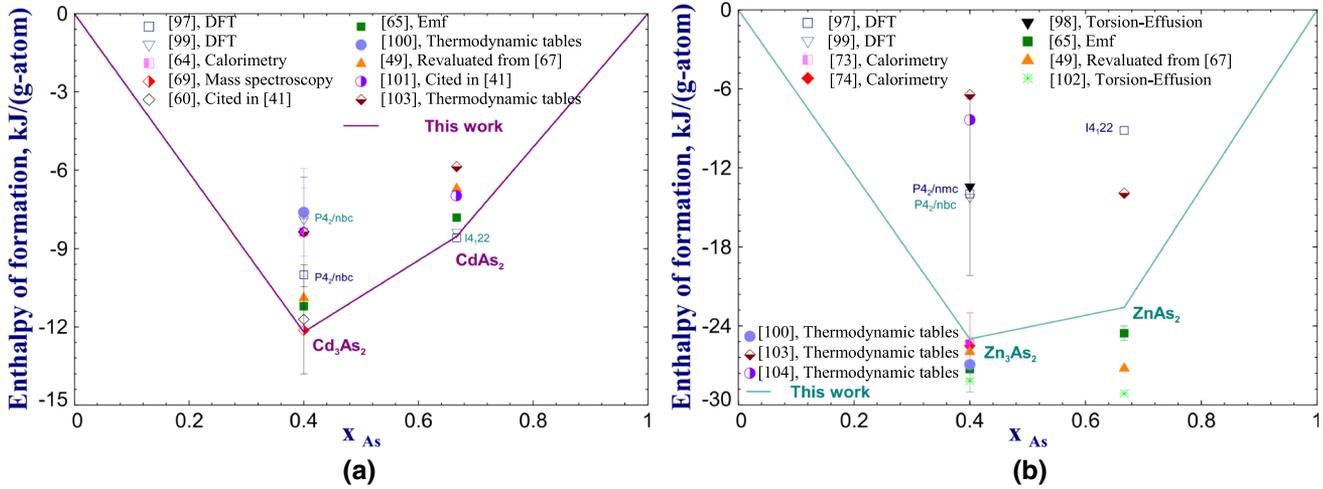
Fig. 1—Enthalpies of formation of intermediate compounds in (*a*) As–Cd system and (*b*) As–Zn system.[97–104]
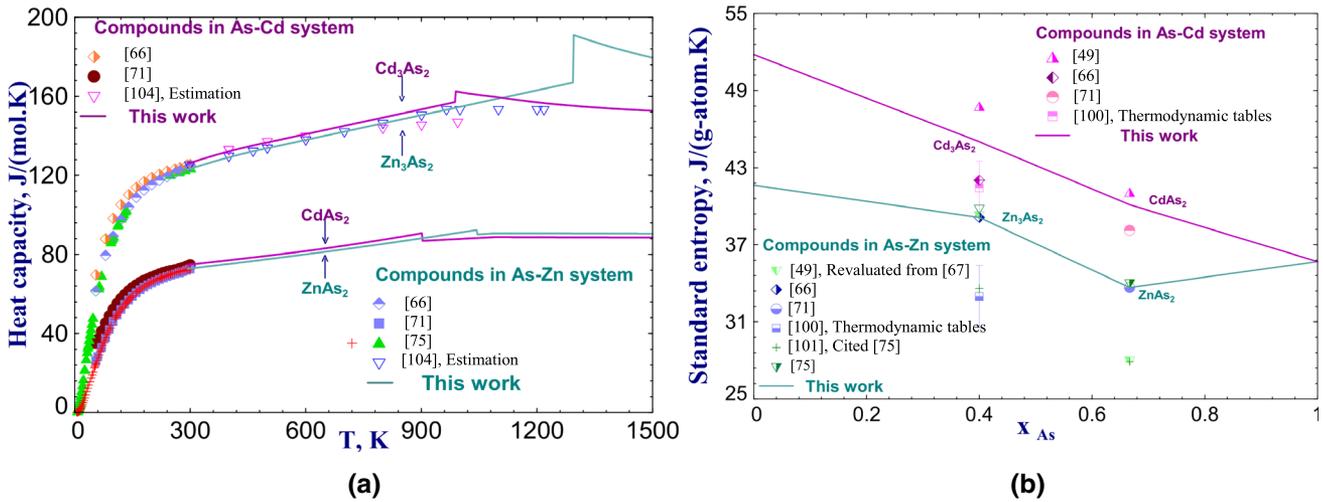
Fig. 2—(*a*) Heat capacities and (*b*) standard entropies of the intermediate compounds in As–Cd and As–Zn systems.

Figures 2(a) and (b) present the heat capacities and the standard entropies of the intermediate compounds respectively. The calculated As–Cd and As–Zn phases diagrams along with the experimental data are presented in Figures 3 and 4. The calculated integral enthalpy and entropy of mixing of liquid in both systems are presented in Figures 5(a) and (b).
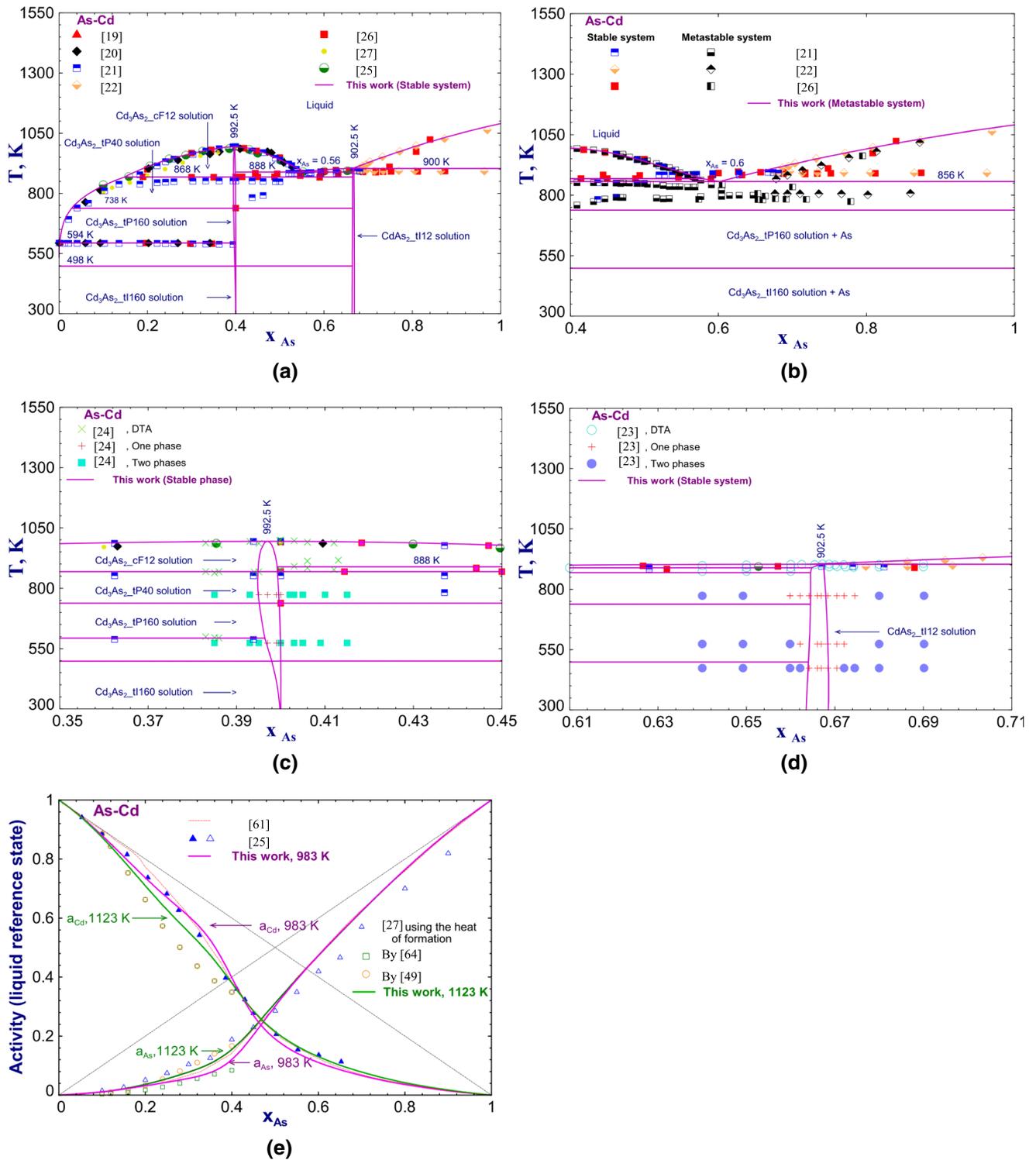
Fig. 3—(a) Calculated As–Cd stable phase diagram, (b) calculated As–Cd metastable phase diagram, (c) calculated homogeneity region of Cd$_3$As$_2$, (d) calculated homogeneity region of CdAs$_2$ and (e) calculated activities of As and Cd in liquid As–Cd melt, with liquid standard states.

At high cooling rates, the formation of solid CdAs$_2$ is difficult because of the viscosity of the liquid, making possible to measure a metastable liquidus in the range of composition from 55 to 75 at. pct As. The experimental studies measuring phase diagram data of As–Cd and As–Zn binary systems are presented in Table II. Details of these studies are also discussed and reviewed in this section.

Fig. 4—(a) Calculated As–Zn phase diagram and (b) calculated homogeneity region of ZnAs₂.

1. As–Cd binary system

a. Cd–Cd₃As₂ subsystem Solid solubility: No information has been reported regarding the solubility of arsenic in solid cadmium. Eutectic: The experiments car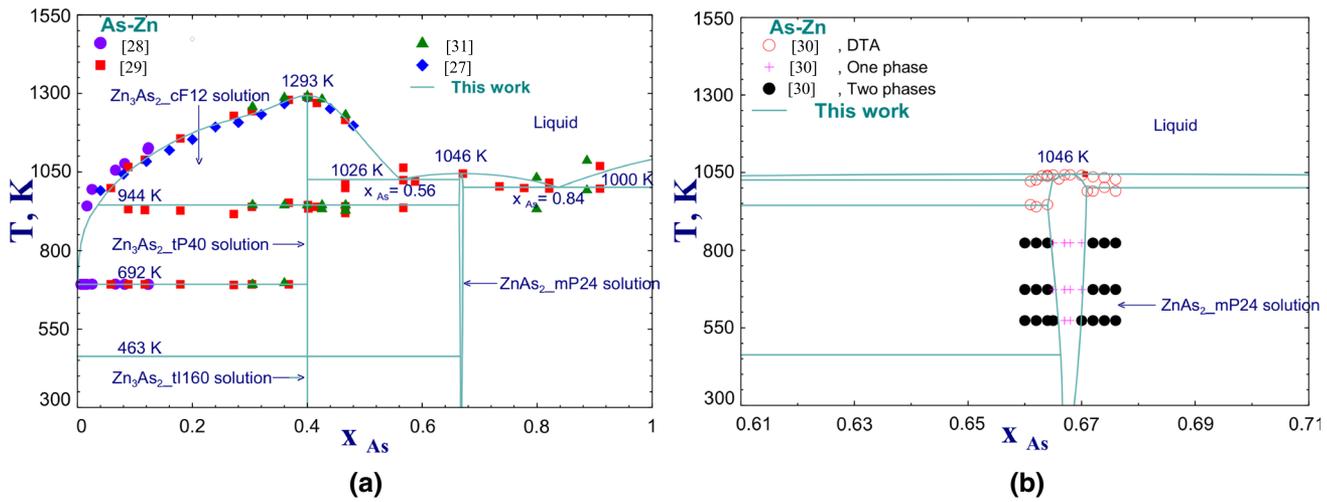ried out by Heycock and Neville[19] show that the melting temperature of cadmium drops by 1 degree after the addition of 0.45 at. pct As. At this composition, a eutectic reaction takes place at a temperature of 592 K to form solid cadmium and Cd_3As_2. This agrees with the eutectic temperatures of 593 K and 592 K measured by Cesaris[20] and Zemczuzny[21] respectively. Liquidus: The liquidus curve of the Cd–Cd₃As subsystem was measured by Cesaris,[20] Zemczuzny[21] and Pruchnik.[26] Calculations of the liquidus curve were also made by Komerek et al.[25] and Yamaguchi et al.[27] The values proposed by these references are all in agreement.

b. Stable and metastable Cd₃As₂–As subsystem In the compositional area between Cd_3As_2 and As, either equilibrium or metastable phase relations realize depending on kinetic limitations of the experiment. There is a tendency for metastable solidification according to Hrubý,[32] and it corresponds to the region of existence of a glassy phase when the formation of $CdAs_2$ is kinetically impeded. Zemczuzny[21] inoculated the liquid with separately prepared crystallites of $CdAs_2$ before cooling to form a stable crystalline $CdAs_2$. Pruchnik[26] also succeeded in making measurements for the stable subsystem. The results of their measurements are presented below.

c. Cd₃As₂–CdAs₂ subsystem (stable solidification) Eutectic: Upon stable cooling, a eutectic reaction takes place at a composition around 56 at. pct As and a

temperature of 883 K to form Cd_3As_2 and $CdAs_2$, according to Zemczuzny.[21] This agrees with the results obtained by Pruchnik.[26] Liquidus: The liquidus curve

of the Cd_3As_2–$CdAs_2$ subsystem was measured by Cesaris,[20] Zemczuzny[21] and Pruchnik.[26] Calculations of the liquidus curve were also made by Komarek et al.[25] The values proposed by these references are all in agreement.

d. CdAs₂–As subsystem (stable crystallization) Solid solubility: No solubility of cadmium in arsenic was reported. Eutectic: During stable cooling, the eutectic reaction to form $CdAs_2$ and solid arsenic takes place at a temperature of 893 K and a composition around 68 at. pct As, according to Gukov et al.[22] This does not agree with Pruchnik[26] who reported a lower temperature of 889 K for the same eutectic reaction, at a composition of approximately 72 at. pct As. Liquidus: Gukov et al.[22] and Pruchnik[26] both measured the liquidus of the $CdAs_2$–As subsystem and their results are not in agreement.

e. Cd₃As₂–As subsystem (unstable solidification) Eutectic: During rapid cooling, a eutectic reaction takes place at a temperature of 799 K and a composition around 62 at. pct As to form Cd_3As_2 and solid arsenic, according to Zemczuzny.[21] This agrees quite well with the values measured by Gukov et al.[22]: a eutectic temperature of 803 K and a composition of 63 at. pct As obtained at a cooling rate of 5 deg./min. However, Pruchnik[26] measured a lower eutectic temperature of 781 K with a eutectic composition of approximately 68 at. pct As at a cooling rate of 10 to 15 deg/min. The measurements by Pruchnik[26] also suggested the formation of a second unstable system, with the formation of an incongruent compound $CdAs_4$ at cooling rate of 5 deg./min. For this system, the eutectic reaction takes place at a temperature of 853 K at a composition around 63 at. pct As to form Cd_3As_2 and $CdAs_4$. Liquidus: The liquidus curve of the $CdAs_2$–As subsystem was measured by Gukov et al.[22] and it is higher than the one measured by Pruchnik.[26]

Table II. As–Cd and As–Zn Phase Diagram Data Reported in the Literature

References	Experimental Methods and Results
As–Cd	
[19]	Raoult's method: determination of the melting temperature of cadmium after arsenic addition
[20]	TA (thermal analysis): determination of the phase diagram up to a composition of 52.7 at. pct As
[21]	TA and metallography: determination of the stable and the metastable phase diagrams, up to a composition of 52.7 at. pct As
[22]	TA, microstructure analysis, XRD and micro-hardness measurements: determination of the phase diagram between compositions of 66 and 100 at. pct As
[23]	DTA (differential thermal analysis), x-ray phase, microstructural analysis, measurements of the microhardness, electrical conductivity and thermo-emf: determination of the region of homogeneity of $CdAs_2$
[24]	DTA, x-ray phase, microstructural analysis, measurements of the microhardness, electrical conductivity and thermo-emf: determination of the region of homogeneity of Cd_3As_2
[25]	emf (Electromotive force) measurements: determination of the liquidus temperatures up to a composition of 45 at. pct As, obtained from the breaks in the emf-temperature curves
[26]	TA, microscopic, XRD and microhardness measurements: determination of the phase diagram between compositions of 20 to 100 at. pct As
[27]	drop calorimetry measurements: determination of the liquidus temperatures up to a composition of 32 at. pct As, obtained from deflection points of heat content vs temperature curves
As–Zn	
[28]	TA and metallography: determination of the phase diagram up to a composition of 12.4 at. pct As
[29]	TA: determination of the phase diagram for all composition range
[30]	DTA, x-ray phase, microstructural analysis, measurements of the microhardness, electrical conductivity and thermo-emf: determination of the region of homogeneity of $ZnAs_2$
[31]	DTA: Determination of the phase diagram between compositions of 40 to 88 at. pct As
[27]	drop calorimetry measurements: determination of the liquidus temperatures up to a composition of 48 at. pct As, obtained from deflection points of heat content vs temperature curves

f. Cd_3As_2 compound Cd_3As_2 Was first reported by Spring[33] who formed the compound using hydraulic pressure and by Granger[34] by heating cadmium in arsenic vapor. Polymorphic transformations: At compositions between 15 and 40 at. pct As, thermal effects were observed by Cesaris[20] around 763 K to 863 K. No conclusions were made regarding these effects. According to Zemczuzny,[21] Cd_3As_2 is dimorphic and its transformation temperature is 851 K. However, according to the experiments of Trzebiatowski et al.,[35] Weglowski and Lukaszewicz[13] and Pietraszko and Lukaszewicz,[36] the compound Cd_3As_2 is polymorphic undergoing three phase transitions at the temperatures presented in Table III. No corresponding enthalpy of transformation was found. Melting temperatures: Measured melting temperatures of Cd_3As_2 are also presented in Table III. Solid solution: According to Bokii et al.,[37] the compound Cd_3As_2 exists within a small composition interval. This was confirmed by the measurements of Lazarev et al.[24] that showed that the phase is unilateral and can dissolve a small amount of cadmium. The boundaries of the region of homogeneity in at. pct of As are 39.5 pct at 773 K, 39.7 pct at 573 K and less than 39.9 pct at 298 K (at. pct As). Polymorphic transformations were not considered in these boundary measurements.

g. $CdAs_2$ compound As reported by Hrubý,[32] $CdAs_2$ exists in three states that can be easily prepared: a stable crystal, a metastable solidified mixture containing Cd_3As_2, $CdAs_2$ and arsenic in a metastable equilibrium state, or a glass in a metastable non-equilibrium state. Polymorphic transformations: According to Ugai and Zyubina[38] and Ugai et al.,[39] $CdAs_2$ undergoes polymorphic transformations, two crystalline and one amorphous. However, the stability range was not reported. No polymorphic transformation was considered in the phase diagram compiled by Okamoto[40] since there is only one crystalline structure of $CdAs_2$ known at atmospheric pressure. Vol and Kagan[41] also did not include any $CdAs_2$ transformation in their compiled phase diagram due to a lack of specific information. Melting temperature: Measured melting temperatures of $CdAs_2$ are presented in Table IV. The experiments of Ugai et al.[39] have shown that glassy $CdAs_2$ decomposes into Cd_3As_2 + As upon heating. Therefore, it undergoes an incongruent melting. Hrubý and Štourač[42] measured an incongruent melting temperature of 891 K and a liquidus temperature of 918 K which, according to Hrubý and Štourač,[42] corresponds approximately to the measurements by Zemczuzny.[21] Solid solution: Marenkin et al.[23] investigated the region of

Table III. Measured and Calculated Temperatures and Heats of Transformation of Cd₃As₂

References	Experimental methods	Temperature, in K (in °C)	$\Delta H_{transformation}$ (kJ/mol)
$Cd_3As_{2(tI160)} \rightleftharpoons Cd_3As_{2(tP160)}$			
[35]	dilatometric method	503.15 (230) ± 3	—
[13]	XRD	503.15 (230) ± 10	—
[24]	DTA	503.15 (230)	—
[36]	XRD	493.15 (220) ± 0.5	—
This Work	—	498.15 (225)	0.1
$Cd_3As_{2(tP160)} \rightleftharpoons Cd_3As_{2(tP40)}$			
[35]	dilatometric method	738.15 (465) ± 3	—
[13]	XRD	738.15 (465) ± 10	—
This Work	—	738.15 (465)	1
$Cd_3As_{2(tP40)} \rightleftharpoons Cd_3As_{2(cF12)}$			
[21]	TA	851.15 (578)	—
[43]	DTA	868.15 (595)	—
[44]	DTA	867.15 (594)	—
[45]	DTA	868.15 (595)	—
[35]	dilatometric method	868.15 (595) ± 3	—
[46]	dilatometric method	851.15 (578)	—
[47]	TA	888.15 (615)	—
[37]	XRD	868.15 (595)	—
[24]	DTA	868.15 (595)	—
[36]	XRD	868.15 (595) ± 1	—
[14]	TA	858.15 (585) ± 1	—
This Work	—	868.15 (595)	38
$Cd_3As_{2(cF12)} \rightleftharpoons Cd_3As_{2(liquid)}$			
[20]	TA	986.15 (713)	—
[21]	TA	994.15 (721)	—
[43]	DTA	994.15 (721)	—
[44]	DTA	977.15 (704)	—
[45]	DTA	992.15 (719)	—
[35]	DTA	994.15 (721) ± 3	—
[46]	dilatometric method	—	74.1*
[47]	TA	989.35 (716.2)	—
[14]	DTA	971.15 (698) ± 2	—
[26]	TA	990.15 (717)	—
[48]	static tensiometric tests	988.15 (715)	—
[49]	Clausius–Clapeyron	—	119.7
This Work	—	992.5 (719.35)	63.6

*Uncertain value, resource no longer available.

homogeneity of CdAs₂ and found that the phase is bilateral. The boundaries of the region of homogeneity in at. pct of As are 65.8 and 67.5 pct at 773 K, 66.3 and 67.2 pct at 573 K and 66.4 and 67.0 pct at 473 K.

2. As–Zn binary system

a. Zn–Zn₃As₂ subsystem Solid solubility: No solubility of arsenic in solid zinc was reported. Eutectic: The eutectic temperature to form solid zinc and Zn_3As_2 is the same as the melting temperature of zinc. It corresponds to 692 K according to the measurements by Friedrich and Leroux[28] and Heike.[29] This temperature agrees with the two values measured by Lazarev et al.[31] Liquidus: The liquidus curve of the Zn–Zn₃As₂ subsystem was measured by Friedrich and Leroux[28] and Heike[29] . Calculations of the liquidus curve were also made by Yamaguchi et al.[27] The values proposed by these references are all in agreement.

b. Zn₃As₂–ZnAs₂ subsystem Eutectic: The eutectic reaction to form Zn_3As_2 and $ZnAs_2$ occurs at a temperature of 1023 K and a composition of 59 at. pct As according to Heike.[29]

c. ZnAs₂ – As subsystem Solid solubility: No solid solubility of zinc in arsenic was reported. Eutectic: The eutectic reaction to form $ZnAs_2$ and solid arsenic occurs at a temperature of 996 K and a composition around 79 at. pct As according to Heike.[29] Liquidus: The liquidus curve of the ZnAs₂–As subsystem was also measured by Heike.[29] The measurements by Lazarev et al.[31] show a liquidus curve about 30 degrees higher than that measured by Heike.[29] Okamoto[53] explains that this disagreement may be due to the difference in the pressure conditions.

Table IV. Measured and Calculated Temperatures and Heats of Fusion of CdAs₂

References	Experimental methods	Temperature, in K (in °C)	ΔH_{fusion} (kJ/mol)
$CdAs_{2(tI12)} \rightleftharpoons CdAs_{2(liquid)}$			
[21]	TA	894.15 (621)	—
[46]	dilatometric method	—	35.2*
[42]	DTA	891.15 (618)	—
[50]	DTA	894.15 (621)	—
[26]	TA	894.15 (621)	—
[48]	static tensiometric tests	897.15 (624)	—
[51]	DTA	900 (626.85)	—
[52]	DTA	898 (624.85)	—
This Work	—	902.5 (629.35)	68.5

*Uncertain value, resource no longer available.

Table V. Measured and Calculated Temperatures and Heats of Transformation of Zn₃As₂

References	Experimental Methods	Temperature, in K (in °C)	$\Delta H_{transformation}$ (kJ/mol)
$Zn_3As_{2(tI160)} \rightleftharpoons Zn_3As_{2(tP40)}$			
[35]	dilatometric method	463.15 (190) ± 3	—
[55]	dilatometric method	463.15 (190) (heating) 433.15 (160) (cooling)	—
[36]	XRD	435.15 (162) ± 0.5	—
This Work	—	463.15 (190)	1
$Zn_3As_{2(tP40)} \rightleftharpoons Zn_3As_{2(cF12)}$			
[29]	TA	945.15 (672)	—
[43]	DTA	943.15 (670)	—
[35]	dilatometric method	945.15 (672) ± 3	—
[13]	XRD	945.15 (672) ± 10	—
[55]	dilatometric method	945.15 (672)	—
[36]	XRD	945.15 (672) ± 1	—
[56]	XRD	932.15 (659) ± 3	—
[44]	DTA	933.15 (660)	—
[57]	DTA extrapolation	929.15 (656)	—
[45]	DTA	943 (670)	—
[14]	TA	924.15 (651)±1	—
[31]	DTA and XRD	945.15 (672)	—
[58]	calculated from[59]	947 (673.85)	37.6
This Work	—	944.15 (671)	39.2
$Zn_3As_{2(cF12)} \rightleftharpoons Zn_3As_{2(liquid)}$			
[29]	TA	1288 (1015)	—
[43]	DTA	1295.15 (1022)	—
[44]	DTA	1288 (1015)	—
[57]	DTA	1288 (1015)	—
[45]	DTA	1295.15 (1022)	—
[46]	dilatometric method	—	92.5*
[49]	Clausius–Clapeyron	—	154.4
[31]	DTA	1288 (1015)	—
This Work	—	1292.5 (1019.35)	72.74

*Uncertain value, resource no longer available.

d. Zn₃As₂ compound Descamps[54] and Spring[33] first reported the formation of Zn_3As_2 by chemical reactions. Polymorphic transformations: Contrary to Cd_3As_2, Zn_3As_2 undergoes only two polymorphic transitions at the temperatures presented in Table V. Melting temperature: The melting temperatures reported for Zn_3As_2 are also presented in Table V. Solid solution: Zn_3As_2 has a very narrow homogeneity range according to Heike.[29] The vapor pressure measurements by Lazarev et al.[31] using the static method confirm that the solubility of

arsenic in the α-Zn_3As_2 does not exceed 5×10^{-4} at. pct.

e. ZnAs₂ compound Melting temperature: Congruent melting temperatures of $ZnAs_2$ are presented in Table VI. Solid solution: Lazarev et al.[30] investigated the region of homogeneity of $ZnAs_2$ and found that the phase is bilateral. The boundaries of the region of homogeneity in at. pct of As are 66.5 and 67.0 pct at 823 K, 66.5 and 67.0 pct at 673 K and 66.66 and 66.8 pct at 573 K.

References	Experimental methods	Temperature, in K (in °C)	$\Delta H_{transformation}$ (kJ/mol)
$ZnAs_{2(mP24)} \rightleftharpoons ZnAs_{2(liquid)}$			
[29]	TA	1044.15 (771)	—
[46]	dilatometric method	—	40.6*
[49]	calculated by method in Ref. [60]	—	85.4
[30]	DTA	1041.5 (768.35)	—
[51]	DTA	1046 (772.85)	—
This Work	—	1045 (771.85)	85.9

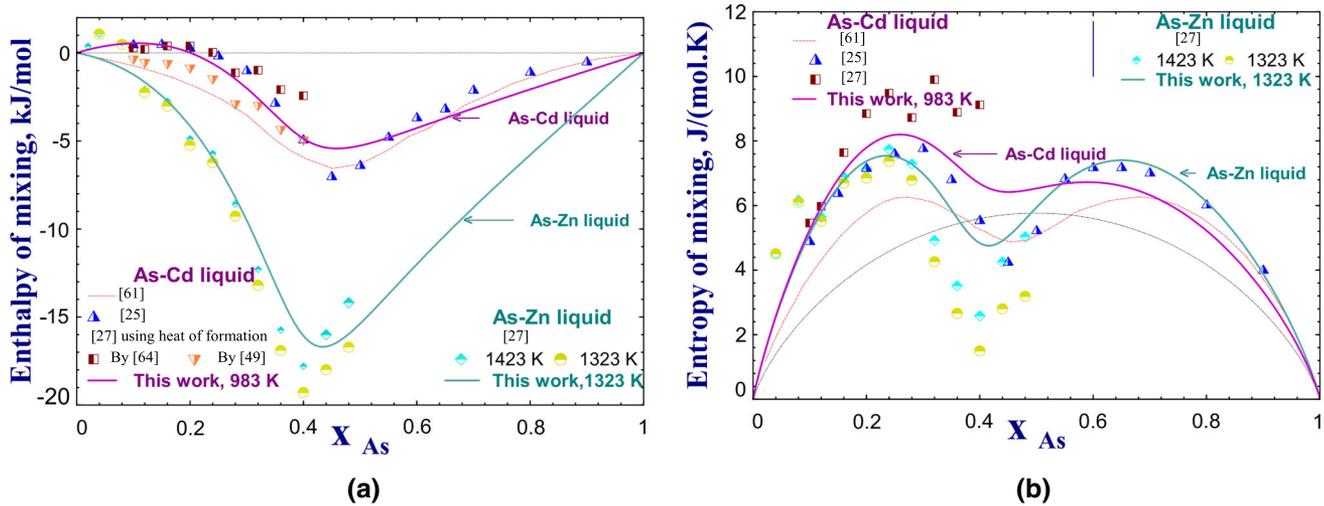*Uncertain value, resource no longer available.

Fig. 5—(a) Calculated integral enthalpy of mixing of liquid in As–Cd and As–Zn systems and (b) calculated integral entropy of mixing of liquid in As–Cd and As–Zn system.

B. Thermodynamic Properties of As–Cd and As–Zn Binary Systems

1. As–Cd liquid

Scheil and Kalkuhl[61] used liquid As–Cd alloys to determine the emf for the cell $Cd_{(l)}|Cd^{2+} + (KCl + LiCl)_{(l)}|$ liquid As–Cd alloys, between 673 K and 1073 K. Points were measured with a heating and cooling rate of 30 deg per hour. Komarek et al.[25] also used liquid As–Cd alloys to determine the emf of the same cell between the liquidus temperature and 1023 K. The measurements were made every 1 to 1.5 K, with heating and cooling rates of 5 to 8 deg per hour. Because of the high vapor pressure of arsenic and cadmium, no measurements could be performed at compositions higher than 67 at. pct As. Extrapolations to pure arsenic were made for the rest of the compositions. The experimental results and the partial molar properties of Cd referred to liquid Cd as the standard state were given. Also, integral molar quantities were derived by Gibbs–Duhem and given for a temperature of 994 K by Scheil and Kalkuhl[61] and for a temperature of 983 K by Komarek et al.[25] In the concentration range of 10 to 40 at. pct As, the heat content of the binary As–Cd system was determined by Yamaguchi et al.[27] using drop calorimetry from 750 K to 1250 K,

and the thermodynamic quantities were derived using the thermodynamic analysis method. The results of Scheil and Kalkuhl[61] and Komarek et al.[25] are in agreement as shown in Figure 5. The obtained activities exhibit negative deviation from Raoult's law. Also, the calculated integral enthalpy of mixing is negative over most compositions. It has a minimum around 45 at. pct As. The curve calculated by Komarek et al.[25] and Yamaguchi et al.[27] show slightly positive values for Cd rich alloys compared to the curve calculated by Scheil and Kalkuhl.[61]

Using mass spectroscopy, Ivanov and Kaller[62] analyzed the composition of vapor in equilibrium with a liquid alloy of composition of 7.4 at. pct As. The measurements were made at temperatures between 726 K and 792 K and revealed the presence of the following ions in the vapor: $Cd^+, As^+, As_2^+, As_4^+$. The heavier Cd_3As_2 and $CdAs_2$ molecules were not detected.

2. As–Zn liquid

Due to the high melting point of Zn_3As_2 and the high vapor pressure of As and Zn, no direct thermodynamic measurements of the As–Zn liquid have been performed. Mikula and Komarek[63] extrapolated the measured emf data of the ternary As–Cd–Zn system to the binary As–Zn to get values of the Gibbs free energy and Zn

activities in the undercooled liquid state for 1023 K and 1123 K. In the concentration range of 4 to 48 at. pct As, the heat content of the binary As–Zn system was determined by Yamaguchi et al.[27] using drop calorimetry from 800 K to 1450 K, and the thermodynamic quantities were derived using the thermodynamic analysis method. Zn activities of Mikula and Komarek[63] and Yamaguchi et al.[27] both exhibit negative deviation from the Raoult's law, just like Cd activities in As–Cd system.

3. Cd₃As₂ compound

Figure 1 shows the available standard enthalpies of formation of Cd₃As₂. Shchukarev et al.[64] reacted Cd₃As₂ with a solution of KBr saturated with bromine, and under the same conditions, also reacted elemental As and Cd with the same solution. A standard enthalpy of formation of − 42 ± 8 kJ/mol was then calculated from the difference between the measured heat of the reactions. Sirota and Sklyarenko[65] measured the emf of the cell Cd |Cd²⁺ + (KCl + LiCl)(l)|Cd₃As₂ + CdAs₂ and the calculated $\Delta H^{\circ}_{formation}$ is − 56 ± 3 kJ/mol. The heat capacity of Cd₃As₂ was measured for low temperatures by Demidenko et al.[66] using vacuum adiabatic calorimetry between 55 K and 300 K. The measured data is presented in Figure 2(a). The standard entropy calculated from these data is also presented in Figure 2(b). Several studies determined the vapor pressure of Cd₃As₂ and Figure 6(a) shows the data from each study. Using the effusion method in Knudsen cells, Nesmeyanov et al.[67] measured the vapor pressure at temperatures between 511 K and 648 K and it was proposed that the vapor contains mainly Cd₃As₂ molecules. However, subsequent studies have proposed another dissociation mechanism. Lyons and Silvestri[68] measured vapor pressure between 707 K and 968 K with a dew-point technique, assuming the compound exists as a monomer in the vapor phase. Lyons and Silvestri[68] also measured vapor pressure between 790 K and 865 K with the direct pressure method with a quartz Bourdon

gauge. From the ratio of the vapor pressure determined by the two methods, it has been deduced that the dissociation takes place incongruently according to the following reaction:

$$Cd_3As_{2(s)} \rightleftharpoons 3Cd_{(g)} + \frac{1}{2}As_{4(g)} \qquad [1]$$
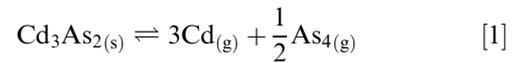
This dissociation reaction was confirmed by Westmore et al.[69] using mass spectroscopy technique. Kalevich et al.[70] also measured vapor pressure of Cd₃As₂ using the isteniscope technique for temperatures between 853 K and 1000 K and using a Bourdon gauge for temperatures between 833 K and 1111 K.

4. CdAs₂ compound

Figure 1 presents the available standard enthalpies of formation of CdAs₂. Sirota and Sklyarenko[65] measured the emf of the cell Cd |Cd²⁺ + (KCl + LiCl)(l)| CdAs₂ + As and the calculated standard enthalpy of formation is − 23.4 ± 0.8 kJ/mol. The heat capacity of CdAs₂ was measured for low temperatures by Danilenko et al.[71] between 55 K and 300 K. The measured data is presented in Figure 2. The standard entropy calculated from these data is also presented in Figure 2. Figure 6(b) shows the measured vapor pressure of CdAs₂. Using a dew-point technique, Lyons and Silvestri[68] measured the vapor pressure at temperatures between 608 K and 888 K. They also used a direct pressure method employing a quartz Bourdon gauge at temperatures in the range of 717 K and 879 K. CdAs₂ is shown to thermally dissociate according to the following reaction:

$$CdAs_{2(s)} \rightleftharpoons \frac{1}{3}Cd_3As_{2(s)} + \frac{1}{3}As_{4(g)} \qquad [2]$$
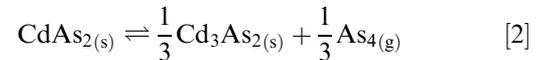
Marenkin et al.[72] also measured the vapor pressure using the static method with a Bourdon quartz manometer.
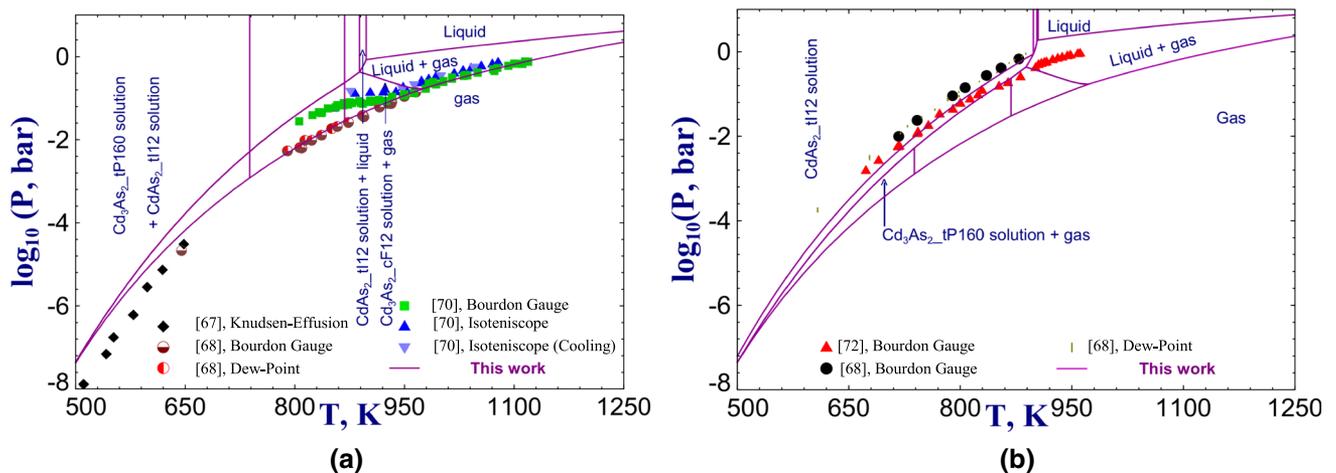

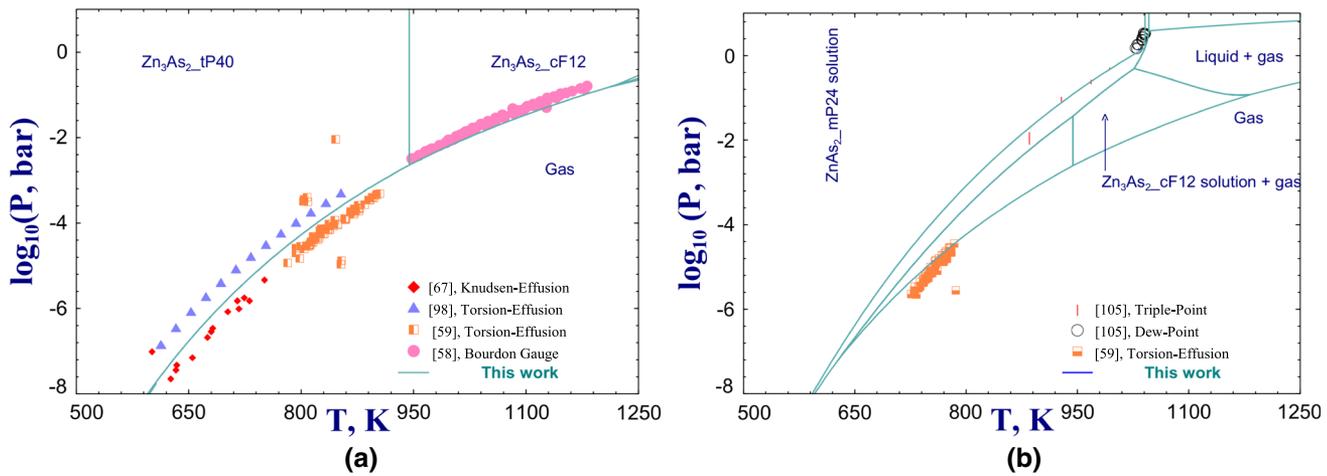Fig. 6—Calculated vapor pressures of (a) Cd₃As₂ and (b) CdAs₂ phases.

Fig. 7—Calculated vapor pressures of (*a*) Zn_3As_2 and (*b*) $ZnAs_2$ phases.

5. Zn_3As_2 compound

The available standard enthalpies of formation of Zn_3As_2 are presented in Figure 1. Natta and Passerini[73] measured the heat of formation of the compound indirectly in a Dewar flask. The heat of dissolution of this compound in dilute hydrochloric acid was measured and Hess's law was used to calculate a value of -126.8 kJ/mol. Ariya et al.[74] repeated the same experiment and calculated a value of -127.6 kJ/mol. Sirota and Sklyarenko[65] measured the emf of the cell $Zn\,|Zn^{2+} + (KCl + LiCl)_{(l)}|Zn_3As_2 + ZnAs_2$ and the calculated standard enthalpy of formation is -136.4 ± 5 kJ/mol. As shown in Figure 2(a), the heat capacities of Zn_3As_2 were measured at low temperatures by Demidenko et al.[66] between 55 K and 300 K and by Gorbunov et al.[75] between 10 K and 300 K using vacuum adiabatic calorimetry. The standard entropies calculated from these data are presented in Figure 2(b). Several studies determined the vapor pressure of Zn_3As_2. Figure 7(a) shows data from each study. Using the effusion method in Knudsen cells, Nesmeyanov et al.[67] measured the vapor pressure at temperatures between 601 K and 751 K and it was proposed that the vapor contains mainly Zn_3As_2 molecules. However, subsequent studies rejected the proposed sublimation mechanism. The vapor pressure of the compound was also measured by Schoonmaker and Lemmerman[76] using torsion-effusion method over a range of temperature from 613 K to 853 K. The proposed congruent decomposition reaction is the following:
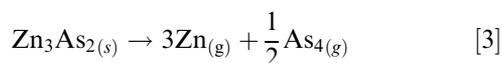
$$Zn_3As_{2(s)} \rightarrow 3Zn_{(g)} + \frac{1}{2}As_{4(g)} \qquad [3]$$

This dissociation reaction was confirmed by Munir[59] using torsion-effusion technique between 782 K and 905 K. Lazarev et al.[31] also measured the vapor pressure of Zn_3As_2 with the static method by use of a quartz Bourdon gauge, for temperatures between 932 K et 954 K. Greenberg et al.[58] also performed the same measurements for temperatures between 947 K to 1181 K.

6. $ZnAs_2$ compound

The available standard enthalpies of formation of $ZnAs_2$ are presented in Figure 1. Sirota and Sklyarenko[65] measured the emf of the cell $Zn\,|Zn^{2+} + (KCl + LiCl)_{(l)}|\,ZnAs_2 + As$ and the calculated standard enthalpy of formation is -73.6 ± 2 kJ/mol. As shown in Figure 2(a), the heat capacities of $ZnAs_2$ were measured at low temperatures by Demidenko et al.[66] between 55 K and 300 K and by Gorbunov et al.[75] between 10 K and 300 K using vacuum adiabatic calorimetry. The standard entropy calculated from these data is also presented in Figure 2(b). Figure 7(b) shows the measured vapor pressure of $ZnAs_2$. Using a dew-point technique, Lyons and Silvestri[68] measured the vapor pressure at temperatures between 885 K and 1032 K. Lyons and Silvestri[68] also used the triple point technique at temperatures in the range of 1029 K and 1043 K. $ZnAs_2$ is shown to thermally dissociate according to the following reaction:
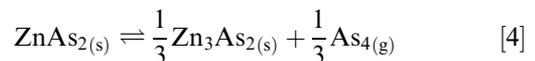
$$ZnAs_{2(s)} \rightleftharpoons \frac{1}{3}Zn_3As_{2(s)} + \frac{1}{3}As_{4(g)} \qquad [4]$$

This dissociation reaction was confirmed by Munir[59] using torsion-effusion technique between 726 K and 786 K.

C. Thermodynamic Assessments of As–Cd and As–Zn Binary Systems in the Literature

No previous assessment was found for the binary As–Cd system. The binary As–Zn system was previously assessed by Dessureault[9] as well as Ghasemi and Johansson,[10] considering stoichiometric compounds. Dessureault[9] modeled the liquid phase using the Quasichemical Model and supposed stoichiometric compounds, using the F*A*I*T system (Formation Analytique Interactive en Thermodynamique), a predecessor of FactSage™.[6–8] Ghasemi and Johansson[10] used the associate-solution model for the liquid phase with three associate species (As, As_2Zn_3, Zn), using the

References	Experimental Methods and Results
Zn_3As_2–Cd_3As_2	
[78]	XRD at room temperature: Suggestion of a phase diagram from room temperature up to 1288 K.
[79]	measurements of the Hall coefficient and resistivity: Suggestion of a phase diagram from room temperature up to 1288 K.
[43]	DTA and XRD: determination of the phase diagram in the temperature range of 867 K and 1288 K.
[44]	DTA and XRD: determination of the phase diagram in the temperature range of 867 K and 1288 K.
[45]	DTA and XRD: determination of the phase diagram in the temperature range of 867 K and 1288 K.
[35]	dilatometric method: determination of the phase diagram in the temperature range of 463 K and 1288 K.
$ZnAs_2$–$CdAs_2$	
[80]	DTA and microhardness measurements: determination of the phase diagram for all composition range.
As–Cd–Zn	
[63]	DTA: determination of several liquid temperatures and their compositions
Zn_3As_2–$CdAs_2$	
[51]	DTA, XRD and microstructural analysis: determination of the phase diagram for all composition range
Zn_3As_2–$CdAs_2$	
[51]	DTA, XRD and microstructural analysis: determination of the phase diagram for all composition range.
Zn_3As_2–$ZnAs_2$–$CdAs_2$–Cd_3As_2	
[51]	prediction of the phase diagram of the liquidus surface

Thermo-Calc software.[77] Using the same software, the Cd–Zn liquid phase was assessed by Zabdyr[11] employing the Redlich–Kister–Muggianu model. The Cd–Zn liquid was also assessed by Min *et al.*[12] using the substitutional solution model. The parameters suggested by Zabdyr[11] for the Cd–Zn are incorporated to the FactSage database and are used in this work to evaluate the ternary As–Cd–Zn, for which we have not found a published thermodynamic assessment.

D. *As–Cd–Zn Ternary Phase Diagram*

Phase equilibria of two quasi-binary sections were established in the As–Cd–Zn system: Zn_3As_2–Cd_3As_2 and $ZnAs_2$–$CdAs_2$. Complete solid solubility between Zn_3As_2 and Cd_3As_2 was suggested at high temperatures. A limited solid solubility was observed in the quasi-binary $ZnAs_2$ and $CdAs_2$, with two types of solid solutions: $Cd_{1-x}Zn_xAs_2$ and $Cd_xZn_{1-x}As_2$. The studies measuring ternary phase diagram data of As–Cd–Zn system are presented in Table VII. Details of these studies are also discussed and reviewed in this section. The calculated Isopleths of the As–Cd–Zn system along with the experimental data are shown in Figure 8.

1. Zn_3As_2–Cd_3As_2 *quasi-binary section*

Solid solubility: A slight decrease of the Cd_3As_2 lattice parameters measured by Zdanowicz *et al.*[78] shows that it can dissolve about 1 pct of Zn_3As_2 below 773 K. Similarly, Zn_3As_2 can also dissolve a small amount of Cd_3As_2. Continuous series of solid solutions: This quasi-binary section forms a continuous series of solid solutions above 738 K. Liquidus and solidus curves measured by Naake and Belcher[43] and Masumoto *et al.*[45] are in good agreement. 25 to 30 deg above the solidus transition, a smaller transition was observed by Castellion and Beegle[44] for $Cd_{3-x}Zn_xAs_2$ specimens for $1.2 < x < 2$, but it was not possible to determine the exact temperature of the transition. The polymorphic transition by Naake and Belcher,[43] Castellion and Beegle,[44] Masumoto *et al.*[45] and Trzebiatowski *et al.*[35] is also in good agreement. Below 738 K, the continuous solid solutions is broken for a certain composition interval because of the formation of a superstructure, identified by Żdanowicz.[78,79] The lattice constant c of the tetragonal cell of the superstructure is equal to twice that of the continuous solid solution The continuous solid solution exists in the ranges of $0.15 \leq x \leq 1.35$ and $2.7 \leq x \leq 3$. It has been found that the superstructure is stable only at low temperatures in the range of $1.35 \leq x \leq 2.7$. Trzebiatowski *et al.*[35] confirmed a reversible phase transition for $Cd_{3-x}Zn_xAs_2$ specimens in the range of $1.35 < x < 1.95$.

2. $ZnAs_2$–$CdAs_2$ *quasi-binary section*

Solid solubility: Ugai *et al.*[81] reported the formation of solid solutions at all concentrations in this quasi-binary section. However, the measurements by Marenkin *et al.*[80] showed that the $ZnAs_2$–$CdAs_2$ quasi-binary section has a simple eutectic with restricted ranges of
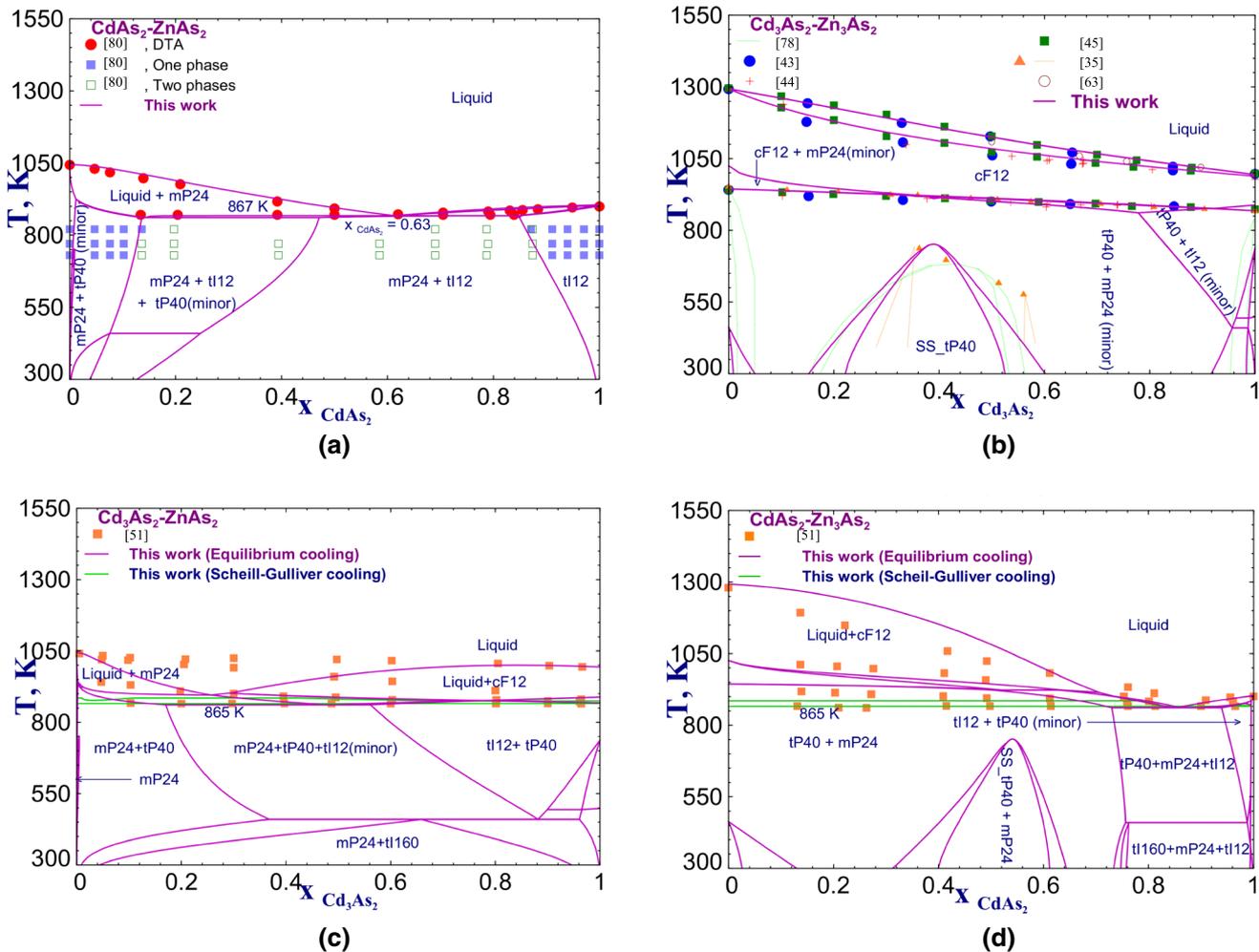
Fig. 8—Calculated Isopleths of the As–Cd–Zn system: (*a*) ZnAs$_2$−CdAs$_2$ join, (*b*) Zn$_3$As$_2$−Cd$_3$As$_2$ join, (*c*) ZnAs$_2$−Cd$_3$As$_2$ join and (*d*) Zn$_3$As$_2$−CdAs$_2$ join.

Cd$_x$Zn$_{1-x}$As$_2$ and Cd$_{1-x}$Zn$_x$As$_2$ solid solutions. Eutectic: According to Marenkin et al.,[80] a eutectic reaction forms Cd$_x$Zn$_{1-x}$As$_2$ and Cd$_{1-x}$Zn$_x$As$_2$ solid solutions at a temperature of 870 K and a composition of 62 at. pct CdAs$_2$. From the liquidus surface constructed by Marenkin et al.,[51] the eutectic reaction takes place at a slightly higher temperature of 879 K.

3. ZnAs$_2$−Cd$_3$As$_2$ and Zn$_3$As$_2$−CdAs$_2$ joins

According to Marenkin et al.,[51] the primary crystallization phase in the ZnAs$_2$−Cd$_3$As$_2$ join is ZnAs$_2$ based solid solutions in the composition range 0 to 15 at. pct Cd$_3$As$_2$ and Cd$_{3-x}$Zn$_x$As$_2$ based solid solutions in the composition range 15 to 100 at. pct Cd$_3$As$_2$. The primary crystallization phase in the Zn$_3$As$_2$−CdAs$_2$ join is Cd$_{3-x}$Zn$_x$As$_2$ based solid solutions in the composition range 0 to 90 at. pct CdAs$_2$ and CdAs$_2$ based solid solutions in the composition range 90 to 100 at. pct CdAs$_2$. Both joins contain a ternary eutectic, which melts at 863 K.

4. Liquidus surface of the ternary As–Cd–Zn system

Based on the measurements presented above, Marenkin et al.[51] constructed the phase diagram of the liquidus surface in the composition region Zn$_3$As$_2$−ZnAs$_2$−CdAs$_2$−Cd$_3$As$_2$. The ternary eutectic in this region has an approximate composition of 26 at. pct Cd + 65 at. pct As + 9 at. pct Zn at a temperature of 863 K. Also, DTA measurements were performed by Mikula and Komarek[63] to determine liquidus temperatures of several ternary alloys.

E. Thermodynamic Properties of As–Cd–Zn Ternary System

1. As–Cd–Zn liquid

Mikula and Komarek[63] used 45 liquid As–Cd–Zn alloys to determine the emf of the cell Zn$_{(l)}$|Zn^{2+} + (KCl + LiCl)$_{(l)}$| liquid As–Cd–Zn alloys. The measurements were made with heating and cooling rates of 8 to 10 deg per hour. From the results, the

iso-activity curves of zinc in the ternary As–Cd–Zn were determined at 1123 K. Thermodynamic functions of formation of solid solutions in the $ZnAs_2-CdAs_2$ and $Zn_3As_2-Cd_3As_2$ quasi-binary sections were also measured using the emf method by Sirota and Smolyarenko.[82] The emf of the following cells were determined, $Zn_xCd_{1-x}|KCl + LiCl + ZnCl_2 + CdCl_2|$ $(Zn_xCd_{1-x})As$ and $Zn_xCd_{1-x}|KCl + LiCl + ZnCl_2 + CdCl_2|$ $(Zn_xCd_{1-x})_3As_2 + (Zn_uCd_{1-u})As_2$. Both $ZnAs_2-CdAs_2$ and $Zn_3As_2-Cd_3As_2$ systems exhibit negative deviation from the Raoult law. Also, the heats of formation determined for the $Zn_3As_2-Cd_3As_2$ system are considerably higher than those for the $ZnAs_2-CdAs_2$ system.

III. THERMODYNAMIC MODELING

All calculations and optimizations in this work were performed with the FactSage[TM] thermochemical software.[6–8] The properties of pure solid and liquid As, Cd and Zn are from SGTE.[83] The properties of gaseous Zn are from JANAF Thermochemical Tables.[84] The properties of the gaseous species As, As_2, As_3, As_4 and Cd are from Degterov et al.[85] and other of their unpublished optimisations and evaluations.

A. Thermodynamic Model for the Liquid Phase

The MQM in the Pair Approximation suggested by Pelton et al.[3,4] was used to model the liquid phases to take into account the short range ordering (SRO). For a liquid binary A–B system, the following pair exchange reaction is considered between the A and B atoms on neighboring sites:

$$(A - A) + (B - B) = 2(A - B); \Delta g_{AB} \quad [5]$$
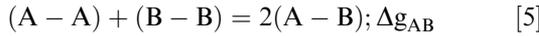
$(i - j)$ is the first nearest neighbor (FNN) atom pairs, and Δg_{AB} is the non-configurational Gibbs energy change for the formation of 2 moles of (A–B) pairs. The pair and the overall mole (site) fractions are defined respectively as:

$$X_{ij} = \frac{n_{ij}}{(n_{AA} + n_{BB} + n_{AB})} \quad [6]$$

$$X_A = \frac{n_A}{(n_A + n_B)} = 1 - X_B \quad [7]$$

n_A, n_B represent the number of moles of A and B, n_{AB} represents the number of moles of pairs (A–B). If the coordination number of A is Z_A, the "coordination equivalent" fraction of A is defined as:

$$Y_A = \frac{Z_A n_A}{Z_A n_A + Z_B n_B} = \frac{Z_A X_A}{Z_A X_A + Z_B X_B} = 1 - Y_B$$
$$= X_{AA} + \frac{X_{AB}}{2} \quad [8]$$

The "coordination equivalent" fraction of B is defined similarly. The Gibbs energy of the binary liquid is given by the following equation:

$$G = (n_A g_A^\circ + n_B g_B^\circ) - T\Delta S^{configuration} + \left(\frac{n_{AB}}{2}\right)\Delta g_{AB} \quad [9]$$

g_A° and g_B° are the molar Gibbs energies of the pure liquid components, and $\Delta S^{configuration}$ is the configurational entropy of mixing given by randomly distributing the (A–A), (B–B) and (A–B) pairs:

$$\Delta S^{configuration} = -R(n_A \ln X_A + n_B \ln X_B)$$
$$- R\left[n_{AA} \ln\left(\frac{X_{AA}}{Y_A^2}\right) + n_{BB} \ln\left(\frac{X_{BB}}{Y_B^2}\right) \right.$$
$$\left. + n_{AB} \ln\left(\frac{X_{AB}}{2Y_A Y_B}\right)\right] \quad [10]$$

The non-configurational Gibbs energy change for the formation of 2 moles of $(A - B)$ pairs is expended in terms of the pair fractions and their expressions for As–Cd and As–Zn systems are as follows:

$$\Delta g_{AsCd} = \Delta g_{AsCd}^\circ + \sum_{i \geq 1} g_{AsCd}^{i0}(X_{AsAs})^i$$
$$+ \sum_{j \geq 1} g_{AsCd}^{0j}(X_{CdCd})^j \quad [11]$$

$$\Delta g_{AsZn} = \Delta g_{AsZn}^\circ + \sum_{i \geq 1} g_{AsZn}^{i0}(X_{AsAs})^i$$
$$+ \sum_{j \geq 1} g_{AsZn}^{0j}(X_{ZnZn})^j \quad [12]$$

Δg_{AsCd}°, Δg_{AsZn}°, g_{AsCd}^{i0}, g_{AsCd}^{0j}, g_{AsZn}^{i0} and g_{AsZn}^{0j} are the temperature dependent model parameters that are optimized in this work.

For a liquid binary A–B system, the coordination numbers can be varied with composition to reproduce the SRO, as given by Eqs. [13] and [14]. The composition of maximum SRO is determined by the ratio Z_B/Z_A:

$$\frac{1}{Z_A} = \frac{1}{Z_{AA}^A}\left(\frac{2n_{AA}}{2n_{AA} + n_{AB}}\right) + \frac{1}{Z_{AB}^A}\left(\frac{2n_{AB}}{2n_{AA} + n_{AB}}\right) \quad [13]$$

$$\frac{1}{Z_B} = \frac{1}{Z_{BB}^B}\left(\frac{2n_{BB}}{2n_{BB} + n_{AB}}\right) + \frac{1}{Z_{BA}^B}\left(\frac{2n_{AB}}{2n_{BB} + n_{AB}}\right) \quad [14]$$

Z_{AA}^A and Z_{AB}^A are the coordination numbers when the nearest neighbours of an A atom are A atoms and B atoms respectively. Z_{BB}^B and Z_{BA}^B are defined similarly. In this work, Z_{AsAs}^{As}, Z_{CdCd}^{Cd} and Z_{ZnZn}^{Zn} are set to be 6 for consistency with previous work. Since maximum SRO

occurs at approximately a composition of 40 at. pct As (composition which corresponds to the minimum of the liquid enthalpy of mixture according to the literature), Z_{AsCd}^{As} and Z_{AsZn}^{As} are set to be 3, and Z_{AsCd}^{Cd} and Z_{AsZn}^{Zn} are set to be 2.

The Cd–Zn binary system was previously assessed by Zabdyr.[11] The liquid phase was modeled using the Bragg–Williams random mixing model in the form of Redlish–Kister polynomial,[86] with ${}^iL_{CdZn}$ as the interaction parameter. The total Gibbs energy and the excess contribution are given by the following equations:

$$G = \left(n_A g_A^\circ + n_B g_B^\circ\right) - T\Delta S^{\text{configuration}} + (n_A + n_B)g^{\text{excess}}$$

[15]

$$g^{\text{excess}} = (X_{Cd}X_{Zn}\sum_{i \geq 0}{}^iL_{CdZn}(X_{Cd} - X_{Zn})^i \quad [16]$$

The configurational entropy of mixing $\Delta S^{\text{configuration}}$ is given by the following equation:

$$\Delta S^{\text{configuration}} = -R(n_A \ln X_A + n_B \ln X_B) \quad [17]$$

Geometric models can be used to estimate the excess Gibbs energy of a ternary system from the parameters of the three binary subsystems.[87] For a given geometric model, the excess Gibbs energy of the ternary system at any composition p is calculated from the binary parameters at points a, b and c. The difference between the models is the placement of these three points. Since the binary excess Gibbs energy in As–Cd and As–Zn systems are large and the parameters depend strongly upon composition, the different models will give very different results. Thus, the choice of points a, b and c is very important to correctly interpolate the ternary system. Since As is chemically different from Cd and Zn, the use of an asymmetric model is more reasonable. In this work, the Kohler–Toop type of extrapolation technique was used to optimize the ternary As–Cd–Zn liquid phase, with arsenic as the asymmetric component, as seen from the following equations:

$$G_{ZnAs}^{\text{excess}} = \frac{(n_{ZnAs})}{2}\left[g_{ZnAs}^{ijk}(X_{ZnZn} + X_{CdZn} + X_{CdCd})^i \right.$$
$$\left. X_{AsAs}^j \left[\frac{Y_{Cd}}{Y_{Zn} + Y_{Cd}}\right]^k\right]$$

[18]

$$G_{CdAs}^{\text{excess}} = \frac{(n_{CdAs})}{2}\left[g_{CdAs}^{ijk}X_{AsAs}^i(X_{CdCd} + X_{CdZn} + X_{ZnZn})^j \right.$$
$$\left. \left[\frac{Y_{Zn}}{Y_{Zn} + Y_{Cd}}\right]^k\right]$$

[19]

$$G_{CdZn}^{\text{excess}} = \frac{(n_{CdZn})}{2}\left[g_{CdZn}^{ijk}\left[\frac{X_{CdCd}}{X_{CdCd} + X_{CdZn} + X_{ZnZn}}\right]^i\left[\frac{X_{ZnZn}}{X_{CdCd} + X_{CdZn} + X_{ZnZn}}\right]^j Y_{As}^k\right]$$

[20]

B. Thermodynamic Model for Solid Solutions

The CEF suggested by Sundman and Ågren[5] is used to model the solid phases. The sub-lattice model for each solid solution in this work is presented in Table VIII and justified below.

1. Solid solutions of $Cd_{3-x}Zn_xAs_2$ phases

The Cd_3As_2 polymorphic forms have related crystal structures, which are based on the anti-fluorite structure (CaF_2). In the ideal Cd_4As_2 anti-fluorite formula, the cations Cd^{2+} occupy the F^- sites and the anions As^{3-} occupy the Ca^{2+} sites. The Cd_3As_2 is cadmium deficient compared to the ideal anti-fluorite formula, missing one-fourth of the Cd atoms and has 25 pct Cd site vacancy, according to Ali et al.[88] and Koumoulis et al.[89] The ordering and the disordering of the vacancies affects the space group to which the crystal belongs. At temperatures higher than 873 K. the Cd ions are disordered and the Cd_3As_2 adopts the ideal anti-fluorite structure, with the $Fm\bar{3}m$ space group. The Cd

Table VIII. Crystallographic Description and Selected Sublattice Model of the Phases in the As–Cd–Zn System used in the Present Study

Phase	Person Symbol	Space group	References	Sub-Lattice Modeling
$Cd_{3-x}Zn_xAs_2(C1)$	cF12	$Fm\bar{3}m$	[13] [14]	$(\mathbf{Cd}, \mathbf{Zn})_3(\mathbf{Va}, \mathbf{Cd})_1(\mathbf{As})_2$
$Cd_{3-x}Zn_xAs_2$ (D5$_9$)	tP40	$P4_2/nmc$	[13] [15]	$(\mathbf{Cd}, \mathbf{Zn})_3(\mathbf{Va}, \mathbf{Cd})_1(\mathbf{As})_2$
$Cd_{3-x}Zn_xAs_2$	tP160	$P4_2/nbc$	[13]	$(\mathbf{Cd}, \mathbf{Zn})_3(\mathbf{Va}, \mathbf{Cd})_1(\mathbf{As})_2$
$Cd_{3-x}Zn_xAs_2$	tI160	$I4_1cd$	[13] [16]	$(\mathbf{Cd}, \mathbf{Zn})_3(\mathbf{Va}, \mathbf{Cd})_1(\mathbf{As})_2$
Super-Structure $Cd_{3-x}Zn_xAs_2$	—	—	—	$(\mathbf{Cd}, \mathbf{Zn})_2(\mathbf{Cd}, \mathbf{Zn})_1(\mathbf{As})_2$
$Cd_{1-x}Zn_xAs_2$	tI12	$I4_122$	[17]	$(\mathbf{Cd}, \mathbf{Zn})_1(\mathbf{Va}, \mathbf{Cd}, \mathbf{As})_1(\mathbf{As}, \mathbf{Va})_2$
$Cd_xZn_{1-x}As_2$	mP24	$P2_1/c$	[18]	$(\mathbf{Zn}, \mathbf{Cd})_1(\mathbf{Va}, \mathbf{As})_1(\mathbf{As}, \mathbf{Zn})_2$

atoms order and shift from the ideal anti-fluorite positions towards the vacancies, resulting in the structures at lower temperatures.[36] According to Lazarev et al.,[24] it can be assumed that the formation of the Cd_3As_2 solid solutions occurs due to the filling of the vacant sites, which explains the deviation from stoichiometry towards the Cd-rich side. Since Cd_3As_2 is an n-type and Zn_3As_2 is a p-type semiconducting material, an n to p transition is expected in $Cd_{3-x}Zn_xAs_2$ solid solutions.[90,91] Based on Hall coefficient and resistivity measurements by Żdanowicz,[79] $Cd_{3-x}Zn_xAs_2$ solid solutions are n-type for $0 \leq x \leq 1.35$ and p-type for $2.7 \leq x \leq 3$ around room temperature. In the range of existence of the superstructure, that is $1.35 \leq x \leq 2.7$, the solid solutions change between n and p-type. Two distinct solid solutions are therefore necessary to model this transition. Using x-ray diffraction analysis, Volodina et al.[92] established that Cd and Zn occupy the same site in $Cd_{3-x}Zn_xAs_2$ solid solutions. Based on the information above, the sub-lattice models used for $Cd_{3-x}Zn_xAs_2$ solid solutions are presented in Table VIII, with Cd occupying the vacant sites to model the deviation from stoichiometry towards the Cd-rich side and Zn occupying the Cd sites. For the $Cd_{3-x}Zn_xAs_2$ superstructure, the sub-lattice model presented in Table VIII is selected considering its composition range reported in the literature.

2. Solid solutions of $Cd_{1-x}Zn_xAs_2$ and $Cd_xZn_{1-x}As_2$ phases

Marenkin et al.[23] suggest that $CdAs_2$ solid solution is formed as a result of both Frenkel and Schottky point defects. Marenkin et al.[93] also determined the structural defects in $CdAs_2$ by investigating the spectra of optical absorption and photoconductivity. Their results that $CdAs_2$ is always enriched in Cd with respect to the stoichiometric composition. The excess Cd occupies an interstitial lattice and vacancies are formed on the As site. Also, it is unlikely that the $CdAs_2$ solid solution has anti-site defects because of the difference in radius between Cd and As. Since the thermal dissociation of $CdAs_2$ releases As atoms, Morozova et al.[94] proposed that As atoms may pass from lattice sites to interstitial positions. Based on impurity photoconductivity spectra measurements, and since Zn and As have similar covalent radius, Morozova et al.[94] suggested that $CdAs_2$-based solid solutions are likely to have anti-site defects, where Zn atoms fill vacancies on As site. However, according to Sanygin et al.,[52] Zn substitution on the As site is very unlikely. Zn is deficient in valence electrons compared to As, and since Zn and Cd are isoelectronic, the Zn in $CdAs_2$-based solid solutions substitutes on the Cd site. Moreover, based on the laser ionization mass spectrometry and electron probe x-ray microanalysis data for $Cd_{0.95}Zn_{0.05}As_2$ solid solution, Zn substitution for Cd is confirmed.

Marenkin et al.[95] explain that for $ZnAs_2$, As atoms may pass from lattice sites to interstitial positions. Also, Zn atoms are likely to form anti-site defects since its covalent radius is closer to that of As, contrary to Cd atoms. Zn vacancies are also possible, but their

concentration must be substantially lower than those of other defects. Unlike $CdAs_2$-based solid solutions, $ZnAs_2$-based solid solutions are interstitial and not substitutional. As explained by Sanygin et al.,[52] Zn substitution by Cd atoms is unfavorable since Zn–As bonds are stronger than Cd–As bonds. This is based on the empirical relationship relating the change in molecular weight to the stability of $II-V_2$ semiconductors. For $Cd_{0.03}Zn_{0.97}As_2$ solid solution, the X-ray diffraction done by Sanygin et al.[52] confirms the presence of interstitial Cd atoms. Investigation of photoconductivity spectra by Morozova et al.[96] also validates that Cd atoms occupy interstices upon the introduction of $ZnAs_2$ into $CdAs_2$. Even though the substitution mechanism of Cd by Zn is not the most favored according to the literature, it was considered in the $Cd_{1-x}Zn_xAs_2$ model selected in the present work in order to be consistent with a mP24 solid solution model already established in the FactSage database. The selected $Cd_{1-x}Zn_xAs_2$ model reproduce very well the ternary data. The sub-lattice models used for $Cd_{1-x}Zn_xAs_2$ and $Cd_xZn_{1-x}As_2$ solid solutions are presented in Table VIII.

IV. RESULTS AND DISCUSSION

The optimization of the thermodynamic parameters was conducted using the FactSage™ thermochemical software. The As–Cd and As–Zn systems are assessed based on the literature data presented in the previous sections, and the optimized thermodynamic model parameters are presented in Table IX. The enthalpies of formation (measurements and DFT) of the different compounds of the binary systems are shown in Figure 1, along with the optimized values from this work. The presented values are normalized per atom in each molecule. There is a large discrepancy in the values suggested by various authors, but the enthalpies of formation of the compounds in the As–Zn system are generally about two times more negative than the values of the compounds in the As–Cd system. Also, the enthalpy of formation per atom selected for Cd_3As_2 and Zn_3As_2 are higher than those of the compounds $CdAs_2$ and $ZnAs_2$ respectively. The transition enthalpies selected in this work and presented in Tables III and V are estimates based on the crystallographic structures of the different phases. The estimated heat capacity (C_p) curves of the intermediate phases are presented in Figure 2(a). Since there are no data measured at higher temperatures, the estimation of the curves was done in two steps. A first estimation was made using the Neumann–Kopp rule which gave slightly higher values than the measured experimental data at 298.15 K. The curves were then shifted down to reproduce the measurements at room temperature. The standard entropies of compounds selected in this work are presented in Figure 2(b). The calculated binary phase diagrams are shown in Figures 3 and 4 below, along with the experimental data. For both As–Cd and As–Zn systems, there is a disagreement in the data reported for arsenic

Table IX. Optimized Thermodynamic Parameters for the As–Cd, As–Zn and As–Cd–Zn (J mol^{-1})

Phases (Model)	Thermodynamic Parameters	References
Liquid (MQM) (**As, Cd, Zn**)(**Va**)	$Z_{AsCd}^{As} = Z_{AsZn}^{As} = 3;\ Z_{AsCd}^{Cd} = Z_{AsZn}^{Zn} = 2;\ Z_{AsAs}^{As} = 2;\ Z_{CdCd}^{Cd} = Z_{ZnZn}^{Zn} = 6$ $\Delta g_{As-Cd} = -16623.6037 + 2.6086T + (23000 - 18.8400)X_{CdCd} + (9.347.8261 - 9.6396T)X_{AsAs}$ $\quad + (-4.8739T)X_{CdCd}^3 + (-3043.4783)X_{AsAs}^3$ $\Delta g_{As-Zn} = (-40534.2885 + 6T) + (36500 - 21.578T)X_{ZnZn}(18900 - 22.1711T$ $\quad + 0.35Tln(T))X_{AsAs} + (-5T)X_{ZnZn}^3 + (-7000)X_{AsAs}^3$ $g_{ZnAs(Cd)}^{011} = -87000$ $g_{AsCd(Zn)}^{101} = 82000$ $g_{ZnAs(Cd)}^{001} = -5.5T$	This work
Liquid (B-W) (Cd, Zn)(Va)	$^0L_{Cd-Zn} = 2792.1666 - 0.1597T$ $^1L_{Cd-Zn} = -19.4 - 0.1373T$ $^2L_{Cd-Zn} = 189.1667$	[11]*
FCC_A1 (B-W) (Cd, Zn)$_1$(Va)$_1$	$^0L_{Cd,Zn:Va} = 15000$	[11]
BCC-A2 (B-W) (Cd, Zn)$_1$(Va)$_3$		[11]
HCP-A3 (B-W) (Cd, Zn)$_1$(Va)$_{0.5}$	$^0L_{Cd,Zn:Va} = 100000$	[11]
cF12(CEF) (Cd, Zn)$_3$(Va, Cd)$_1$(As)$_2$	$^0L_{Cd,Zn:Va} = (17845.8 - 0.639T)$ $^1L_{Cd,Zn:Va} = (-7167.4 + 7.955T)$ $^0G_{Cd:Va:As} = -21900 + 43.618T + 3GHSER_{Cd} + 2GHSER_{As}$ $^0G_{Zn:Va:As} = -84800 + 43.037T + 3GHSER_{Zn} + 2GHSER_{As}$ $^0G_{Cd:Cd:As} = -6900 + 43.6184 + 4GHSER_{Cd} + 2GHSER_{As}$ $^0G_{Zn:Cd:As} = -69800 + 43.037T + 3GHSER_{Cd} + GHSER_{Cd} + 2GHSER_{As}$ $^0L_{Cd,Zn:Va:As} = -14000$	This work
tP40(CEF) (Cd, Zn)$_3$(Va , Cd)$_1$(As)$_2$	$^0G_{Cd:Va:As} = -59900 - 0.153T + 3GHSER_{Cd} + 2GHSER_{As}$ $^0G_{Zn:Va:As} = -124000 + 1.512T + 3GHSER_{Zn} + 2GHSER_{As}$ $^0G_{Cd:Cd:As} = -44900 - 51.953T + 4GHSER_{Cd} + 2GHSER_{As}$ $^0G_{Zn:Cd:As} = -109000 - 51.800T + 3GHSER_{Zn} + GHSER_{Cd} + 2GHSER_{As}$ $^0L_{Cd,Zn:Va:As} = -15000$	This work
SS_tP40(CEF) (**Cd, Zn**)$_2$(**Cd, Zn**)$_1$(**As**)$_2$	$^0G_{Cd:Cd:Va:As} = -21900 + 43.618T + 3GHSER_{Cd} + 2GHSER_{As}$ $^0G_{Cd:Zn:Va:As} = -26900 - 226.779T + 2GHSER_{Cd}$ $\quad + GHSER_{Zn} + 2GHSER_{As}$ $^0G_{Zn:Cd:Va:As} = -69600 - 188.869T + 2GHSER_{Zn} + GHSER_{Cd} - GHSER_{Zn}$ $^0G_{Zn:Zn:Va:As} = -84800 + 43.037T + 3GHSER_{Zn} + 2GHSER_{As}$ $^0L_{Zn:Cd,Zn:Va:As} = 2505$	This work
tP160(CEF) (**Cd, Zn**)$_3$(**Va, Cd**)$_1$(**As**)$_2$	$^0G_{Cd:Va:As} = -60900 - 1.508T + 3GHSER_{Cd} + 2GHSER_{As}$ $^0G_{Zn:Va:As} = -124000 + 1.512T + 3GHSER_{Zn} + 2GHSER_{As}$ $^0G_{Cd:Cd:As} = -45900 - 53.308 + 4GHSER_{Cd} + 2GHSER_{As}$ $^0G_{Zn:Cd:As} = -109000 - 50.288T + 3GHSER_{Zn} + GHSER_{Cd} + 2GHSER_{As}$	This work
tI160(CEF) (**Cd, Zn**)$_3$(**Va, Cd**)$_1$(**As**)$_2$	$^0G_{Cd:Va:As} = -61000 - 1.708T + 3GHSER_{Cd} + 2GHSER_{As}$ $^0G_{Zn:Va:As} = -125000 - 0.648T + 3GHSER_{Zn} + 2GHSER_{As}$ $^0G_{Cd:Cd:As} = -46000 - 53.508T + 4GHSER_{Cd} + 2GHSER_{As}$ $^0G_{Zn:Cd:As} = -110000 - 52.448T + 3GHSER_{Zn} + GHSER_{Cd} + 2GHSER_{As}$	This work

Table IX. continued

Phases (Model)	Thermodynamic Parameters	References
tI12(CEF) $(\mathbf{Cd}, \mathbf{Zn})_1 (\mathbf{Va}, \mathbf{Cd}, \mathbf{As})_1 (\mathbf{As}, \mathbf{Va})_2$	${}^0G_{Cd:Va:As} = -25600 - 2.833T + GHSER_{Cd} + 2GHSER_{As}$ ${}^0G_{Cd:Va:Va} = 70000 + GHSER_{Cd}$ ${}^0G_{Cd:Cd:As} = -15600 - 2.833T + 2GHSER_{Cd} + 2GHSER_{As}$ ${}^0G_{Cd:Cd:Va} = 90000 - 51.8T + 2GHSER_{Cd}$ ${}^0G_{Cd:As:As} = 5400 - 116.319T + GHSER_{Cd} + 3GHSER_{As}$ ${}^0G_{Cd:As:Va} = 64400 - 44.940T + GHSER_{Cd} + GHSER_{As}$ ${}^0G_{Zn:Va:As} = -55300 - 12.009T + GHSER_{Zn} + 2GHSER_{As}$ ${}^0G_{Zn:Va:Va} = 100000 + 41.63T + GHSER_{Zn}$ ${}^0G_{Zn:Cd:As} = -2600 - 51.8T + GHSER_{Zn} + GHSER_{Cd}$ ${}^0G_{Zn:Cd:Va} = 60000 + GHSER_{Cd} + GHSER_{Zn}$ ${}^0G_{Zn:As:As} = 7200 + 12.009T + GHSER_{Zn} + 3GHSER_{As}$ ${}^0G_{Zn:As:Va} = 22200 + 59.37T + GHSER_{Zn} + GHSER_{As}$ ${}^0L_{Cd:Va,As:As} = (-30000 + 20.89T)$ ${}^0L_{Cd:Va,Cd:As} = (-28000 + 17.89T)$ ${}^0L_{Cd,Zn:Va:As} = -1500$	This work
mP24(CEF) $(Zn, Cd)_1 (Va, As)_1 (As, Zn)_2$	${}^0G_{Zn:Va:As} = -67800 + 12.009T + GHSER_{Zn} + 2GHSER_{As}$ ${}^0G_{Zn:Va:Zn} = 25000 + 3GHSER_{Zn}$ ${}^0G_{Zn:As:As} = -47800 - 113.009T + GHSER_{Zn} + 3GHSER_{As}$ ${}^0G_{Zn:As:Zn} = 90000 + 3GHSER_{Zn} + GHSER_{As}$ ${}^0G_{Cd:Va:As} = -15600 + 2.833T + GHSER_{Cd} + 2GHSER_{As}$ ${}^0G_{Cd:Va:Zn} = 70000 + 2GHSER_{Zn} + GHSER_{Cd}$ ${}^0G_{Cd:As:As} = 24400 - 38.523T + GHSER_{Cd} + 3GHSER_{As}$ ${}^0G_{Cd:As:Zn} = 70000 + GHSER_{Cd} + GHSER_{As} + 2GHSER_{Zn}$ ${}^0L_{Zn:Va,As:Zn} = (-75000 + 27.9855T)$ ${}^0L_{Zn:Va,As:As} = (-18000 + 25.2002T)$ ${}^0L_{Zn,Cd:Va:As} = (-5000 + 9.8619T)$	This work

*Parameters converted according to the MQM.

rich alloys, probably due to the high vapor pressure of these alloys. For As–Cd system, arsenic liquidus data in the stable and the metastable systems by the same authors do not match due to the rate of heating and cooling used in each experiment are shown in Figure 3(b).

To measure data for the stable As–Cd phase diagram, slower rates were used by Pruchnik[26] and Gukov,[22] and higher rates were used to measure data for the metastable phase diagram. To optimize the liquid parameters in the As–Cd system, the stable phase diagram data as well as the activity data were considered. The Cd activity in liquid As–Cd melt by Komarek et al.[25] as well as Scheil and Kalkuhl[61] are directly obtained from emf measurements. However, only the data from Komarek et al.[25] was used to optimize the liquid phase since it was obtained using a slower heating rate and thus considered more reliable. The calculated As–Cd phase diagram reproduces most experimental data but does not completely fit the measured data at high arsenic content. Because of the disagreement between the different authors and since no activity data is available for arsenic rich alloys, the optimized parameters for the liquid phase at high arsenic compositions has a significant uncertainty. To best reproduce phase diagram data at high arsenic content, a peritectic temperature of 900 K had to be selected for $CdAs_2$–As subsystem instead of the slightly lower eutectic temperature of 893 K reported by Gukov et al.[22] or 889 K by Pruchnik.[26] $CdAs_2$ is then incongruent in this work with a melting point slightly higher than the reported measurements for the crystalline form shown in Table IV. Also, the calculated homogeneity range is narrower than what was measured by Marenkin et al.[23] in order to best reproduce the rest of the phase diagram data. The Cd_3As_2 compound is congruent, with an optimized melting point of 992.5 K. The non-stoichiometry of Cd_3As_2 is unilateral and the existence of the different polymorphic forms causes a slight deviation of the stoichiometric composition of 40 at. pct As, thus giving a "banana shape" that tends towards cadmium at higher temperatures. The stoichiometric deviation starts from a temperature of 572 K, reaching the largest deviation of 0.3 at. pct As towards Cd at the melting point. The calculated As–Zn phase diagram reproduce most experimental data as shown in Figure 4. Both $ZnAs_2$ and Zn_3As_2 have congruent melting temperatures of 1046 K and 1293 K respectively. The compound Zn_3As_2 is considered stoichiometric in this work because no homogeneity range data is reported in the literature. The emf measurements performed by Mikula and Komarek[63] were scattered, and the extrapolation of these measurements to predict Zn activity was not considered reliable enough to use in the optimization of the liquid phase. Since there are no other reliable thermodynamic measurements for the liquid phase, only phase diagram data was used for the optimization of this system.

For both As–Cd and As–Zn systems, Yamaguchi et al.[27] did not report the measured heat content in their paper, but only the thermodynamic quantities derived. Moreover, because of the significant dependence of the results on the chosen heat of formation of the compounds and the uncertainty of the method employed in the calculations, the proposed thermodynamic data by Yamaguchi et al.[27] were not directly considered in optimizing the parameters. However, the reported data was used as a reference to compare As–Cd and As–Zn systems. Figure 5(a) compares the calculated enthalpy of mixing of the liquids in each binary system. The shape of the calculated curves in both systems is very similar, positive for high metal composition and very negative around the SRO compositions. The negative deviations from ideality in the liquid As–Zn solution are more pronounced than for the liquid As–Cd solution. Komarek et al.[25] suggested a curve minimum at 48 at. pct As for the enthalpy of mixing of the liquid in the As–Cd system, which is consistent with the minimum suggested by Scheil and Kalkuhl.[61] It can also be seen from the same figure that the enthalpy of mixing of the liquid in the As–Zn system has a minimum of 40 at. pct As according to Yamaguchi et al.[27] In this work, the same coordination numbers were selected in both systems to fix the composition of maximum SRO in As–Cd and As–Zn liquid phases. By setting Z_{AsCd}^{As} and Z_{AsZn}^{As} to 3, and Z_{AsCd}^{Cd} and Z_{AsZn}^{Zn} to 2, the calculated integral enthalpy of mixing of Cd–As system has a minimum around what was measured. Small coordination numbers were selected since the reported enthalpy of mixing curves of the two systems seems to be very sharp. As shown in Figure 5, the integral enthalpy of mixing curves have a "V" shape and the integral entropy of mixing curves have an "m" shape. This is due to the highly ordered liquid phases, which can be explained by the large differences of electronegativity between As (2.18) and the metals Cd (1.69) and Zn (1.65). To optimize the liquid phases of As–Cd and As–Zn systems, parameters using the same indices are necessary in both systems as shown in Table IX. Also, because the liquid phase of As–Zn system is more stable compared to that of As–Cd system, the optimized parameters of liquid As–Zn are about 2.4 times higher. The high stability of the As–Zn liquid phase implies large parameter values to describe the excess Gibbs energy. Because of the large parameter values used for the T-dependent term for g_{AsZn}^{10} shown in Table IX, the model predicts a miscibility gap above 5500 K. To correct the excess Gibbs energy of the liquid phases at high temperatures, the addition of a $CTln(T)$ term for the said term is necessary to avoid the formation of an inverted

The predicted vapor pressures of the intermediate compounds are compared to the experimental data in Figures 6 and 7. For the calculated vapor pressure of Cd_3As_2, the equilibrium includes $CdAs_2$ phase (tI12) because of the deviation from stoichiometry at high temperatures discussed previously. Also, there is a disagreement in the data for Zn_3As_2. According to Greenberg et al.,[58] the difference is probably due to a non-stoichiometric sublimation.

The ternary As–Cd–Zn liquid phase is modeled based on the literature data presented in the previous sections using the Kohler–Toop interpolation. Three ternary parameters, presented in Table IX, were necessary to reproduce more accurately the experimental data. Two large enthalpy terms of opposites signs are used to balance out for a more precise description of the ternary liquid phase. Calculated isopleths of the ternary system are shown in Figure 8 and compared with the experimental data. The different phases are identified with their Pearson symbols. Some phases are present at equilibrium in minor quantities and are identified in the Figures with "(minor)". The calculated $ZnAs_2$–$CdAs_2$ and Zn_3As_2–Cd_3As_2 quasi-binary sections are in good agreement with the experimental data. The calculated eutectic temperature is 867 K with a eutectic composition 63 at. pct $CdAs_2$. For the pseudo-binary Zn_3As_2–Cd_3As_2, tI12 and mP24 solid solutions were found in the phase equilibrium in minor quantities. The superstructure (SS tP40) that breaks the continuous $Cd_{3-x}Zn_xAs_2$ solid solutions at low temperatures is also represented.

As evident from Figure 8, the liquidus in $ZnAs_2$–Cd_3As_2 and Zn_3As_2–$CdAs_2$ joins are not well predicted by the model. Even if the optimized eutectic temperature corresponds to the value measured by Marenkin et al.,[51] the calculated $ZnAs_2$ liquidus for the $ZnAs_2$–Cd_3As_2 system is lower than the experimental data, and the calculated Zn_3As_2 liquidus in the $CdAs_2$–Zn_3As_2 system is higher than the experimental data. Marenkin et al.[51] characterized the samples with DTA using double-walled graphited silica tubes to prevent reaction between the melt and silica. Not enough information was provided on the conditions of the DTA analysis. The samples were also characterized by x-ray powder diffraction (XRD) and microstructural analysis. Considering the tendency of the liquids to be vitreous, the measurements performed by Marenkin et al.[51] may have numerous uncertainties. Also, it is likely that the chosen model is not the best suited to describe the vitreousness of the liquids of the two joins $ZnAs_2$–Cd_3As_2 and $CdAs_2$–Zn_3As_2, which explains the difference between the predictions of the model and the measurements by Marenkin et al.[51] The erroneous prediction of these two joins can be explained by the ability of arsenic to be multivalent. In M_3As_2 and MAs_2 (M = Cd, Zn), arsenic forms distinct chemical bonds because of its different valence states. When arsenic is monovalent (As^-), each atom forms two single bonds that results in one-dimensional chains. Thus, in MAs_2, arsenic forms an anionic substructure following the Zintl–Klemm concept, resulting in infinite helical arsenic chains, with tetrahedrally coordinated Cd, Zn and As[105–107] As_4^{4-} helices were found by Cervinka and Hrubý[17] in crystalline $CdAs_2$, and As_8^{8-} helices were found by Fleet[18] in $ZnAs_2$. The structure of glassy $CdAs_2$ has not been investigated yet but it should be similar to crystalline $CdAs_2$ with a lack of symmetry and periodicity.[108] When arsenic is trivalent arsenic (As^{3-}), as found in M_3As_2, no direct chemical bonds are formed between arsenic atoms.[105] Additionally, the volatilization of elemental arsenic under saturated vapor conditions corresponds to $4As_{(s)} \rightleftharpoons As_{4(g)}$. Other arsenic molecular forms are present under unsaturated vapor conditions ($As_{3(g)}$, $As_{2(g)}$, $As_{(g)}$), with $As_{4(g)}$ remaining as the predominant phase. As the temperature increases, $As_{4(g)}$ decomposes to form mainly $As_{2(g)}$.[109–111] Since the model used in this work does not consider the complex bonding networks of arsenic, the liquidus in $ZnAs_2$–Cd_3As_2 and Zn_3As_2–$CdAs_2$ joins are not well predicted. The presence of arsenic other than the monomeric form may have to be considered by the model for a more satisfactory prediction of the ternary liquidus surface, even if the binary subsystems are well reproduced by the proposed model. Also, DTA measurements were recorded over the entire composition range at the eutectic temperature in both $ZnAs_2$–Cd_3As_2 and Zn_3As_2–$CdAs_2$ systems. However, the two joins calculated at equilibrium conditions show
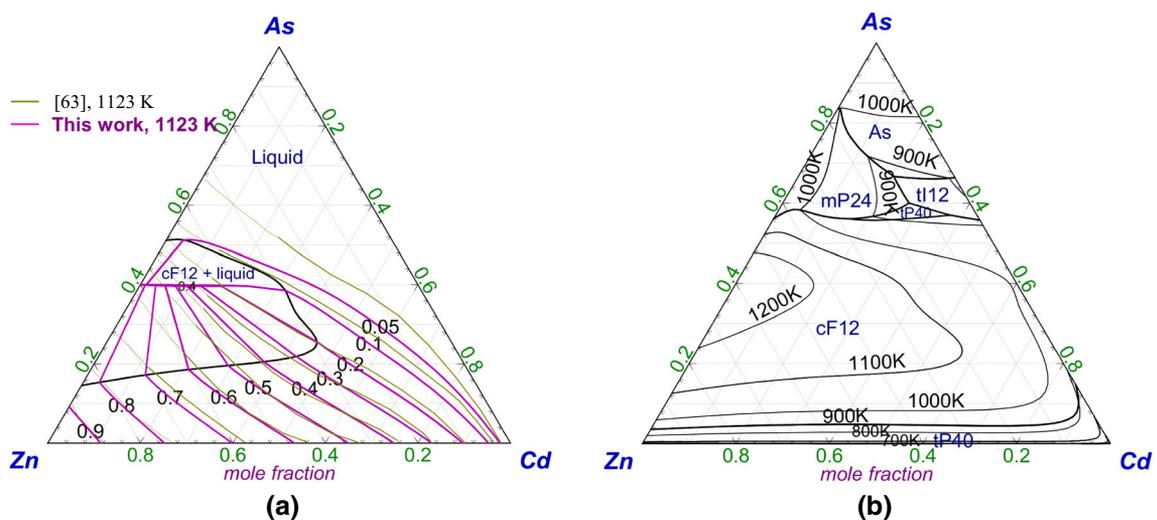

Fig. 9—(a) Calculated isothermal section of the As–Cd–Zn system at 1123 K along with the calculated and the experimental liquid Zn iso-activity curves and (b) predicted liquidus projection.

Table X. Summary of Calculated Invariant Reactions Involving the Liquid Phase in the Ternary As − Cd − Zn system

Reactions			
At. Pct As	At. Pct Cd	At. Pct Zn	Temperatures [K (°C)]
Liquid + As ⇌ tI12 + mP24			
0.666	0.205	0.1290	867.16 (594.01)
Liquid ⇌ mP24 + tP40 + tI12			
0.600	0.270	0.129	860.88 (587.73)
Liquid + mP24 + cF12 ⇌ tP40			
0561	0.162	0.277	922.31 (649.16)
Liquid + cF12 ⇌ tP40 + tI12			
0.570	0.373	0.057	875.97 (602.82)

that the eutectic at 865 K does not extend to all compositions. It is likely that the conditions for measuring the data points approached those of Scheil–Gulliver cooling, represented by the blue curves in the figures. This type of cooling implies that the solid phases no longer react with the liquid phase and remain unchanged once precipitated. The Gibbs energy change of the following pair-exchange reaction $Cd_3As_2 + ZnAs_2 \rightleftharpoons Zn_3As_2 + CdAs_2$ is positive but quite low (a little less than 50 kJ). This explains the absence of a miscibility gap in the $Cd_3As_2-ZnAs_2-Zn_3As_2-CdAs_2$ system. The isotherm at 1123 K is shown in Figure 9 along with the Zn iso-activity curves in the liquid state. The calculated curves are in agreement with the experimental curves by Mikula *et al.*[63] A summary of the invariant reactions involving four-phase intersection points with liquid in the ternary As–Cs–Zn system is presented in Table X.

V. CONCLUSIONS

To ensure the viability of smelters in the future, the use of arsenic-rich concentrates should be considered. The challenge with using this type of concentrate is the reduction of arsenic and cadmium emissions caused by the smelting process. The development of thermodynamic models and their associated databases presented in this work is essential to understand the interaction of arsenic with other metals. To obtain thermodynamic model parameters for As–Cd and As–Zn binary systems, the thermodynamic information available in the literature was critically evaluated and optimized in this work. Both binary systems are highly ordered. To describe the SRO, the MQM in the Pair Approximation was used to model the liquid phase, and the CEF was used to model the solid solutions. The calculated phase diagrams and thermodynamic properties are accurate in describing all the reliable experimental data in both binary systems. Using the Kohler–Toop interpolation, the As–Cd–Zn ternary system was also assessed. It was not possible to reproduce the ternary As–Cd–Zn liquidus surface over the entire composition and temperature ranges with a relatively small number of parameters. $ZnAs_2-CdAs_2$ and $Zn_3As_2-Cd_3As_2$ joins

are correctly reproduced. However, the liquidus of the $ZnAs_2-Cd_3As_2$ and $Zn_3As_2-CdAs_2$ joins are less satisfactory even if the eutectic temperature was optimized. Since the aim is to generate a database which describes the thermodynamic interaction of arsenic with transition metals found in complex concentrates, it is essential to consider the complexity of the behavior of arsenic. To comply with the standard CALPHAD approach, the model used in this work considers liquid arsenic only in its monomeric form. In order to improve the model, it may be necessary to consider more closely the various polymeric forms of liquid arsenic.

CONFLICT OF INTEREST

The authors declare that they have no conflict of interest.

REFERENCES

1. B.J. Alloway and A.P. Jackson: *Sci. Tot. Environ.*, 1991, vol. 100, pp. 151–76.
2. T.O. Llewellyn, *Cadmium (Materials Flow)*, Department of the Interior. Bureau of Mines, 1994.
3. A.D. Pelton, S.A. Degterov, G. Eriksson, C. Robelin, and Y. Dessureault: *Metall. Mater. Trans. B.*, 2000, vol. 31B, pp. 651–59.
4. A.D. Pelton and P. Chartrand: *Metall. Mater. Trans. A.*, 2001, vol. 32B, pp. 1355–60.
5. B. Sundman and J. Ågren: *J. Phys. Chem. Solids*, 1981, vol. 42, pp. 297–301.
6. C.W. Bale, P. Chartrand, S.A. Degterov, G. Eriksson, K. Hack, R.B. Mahfoud, J. Melançon, and S. Petersen: *Calphad*, 2002, vol. 26, pp. 189–228.
7. C.W. Bale, E. Bélisle, P. Chartrand, S.A. Decterov, G. Eriksson, K. Hack, L.-H. Jung, Y.-B. Kang, J. Melançon, A.D. Pelton, C. Robelin, and S. Petersen: *Calphad*, 2009, vol. 33, pp. 295–311.
8. C.W. Bale, E. Bélisle, P. Chartrand, S.A. Decterov, G. Eriksson, A. Gheribi, K. Hack, I.-H. Jung, Y.-B. Kang, J. Melançon, A.D. Pelton, S. Petersen, C. Robelin, J. Sangster, P. Spencer, and M.-A.V. Ende: *Calphad*, 2016, vol. 55, pp. 1–9.
9. Y. Dessureault, *Modelisation thermodynamique du smeltage du plomb dans un haut fourneau*, Génie métallurgique, Polytechnique, Montréal, 1994.
10. M. Ghasemi and J. Johansson: *J. Alloys Compd.*, 2015, vol. 638, pp. 95–102.
11. L.A. Zabdyr: *Calphad*, 1997, vol. 21, pp. 349–58.
12. S. Min, W.G. Jung, and J. Lee: *Met. Mater. Int.*, 2007, vol. 13, pp. 421–25.
13. S. Weglowski and K. Lukaszewicz: *Bull. Acad. Pol. Sci. Set. Sci. Chim.*, 1968, vol. 16, pp. 177–82.
14. C.W.F.T. Pistorius: *High Temp. High Press.*, 1975, vol. 7, pp. 441–49.
15. M.V. Stackelberg and R. Paulus: *Z. Phys. Chem. B*, 1935, vol. 28, pp. 427–60.
16. G.A. Steigmann and J. Goodyear: *Acta Crystallogr. B*, 1968, vol. 24, pp. 1062–67.
17. L. Cervinka and A. Hrubý: *Acta Crystallogr. B*, 1970, vol. 26, pp. 457–58.
18. M.E. Fleet: *Acta Crystallogr. Sect. B Struct. Crystallogr. Cryst. Chem.*, 1974, vol. 30, pp. 122–26.
19. C.T. Heycock and F.H. Neville: *J. Chem. Soc.*, 1892, vol. 61, p. 899.
20. P.D. Cesaris: *Rend. Soc. Chim. Ital. (Rome)*, 1912, vol. 4, pp. 196–99.
21. S.F. Zemczuzny: *Int. Z. Metallogr.*, 1913, vol. 4, pp. 228–47.
22. O.Y. Gukov, Y.A. Ugai, V.R. Pshestanchik, E.G. Gonchrov, and N.V. Pakhomova: *Inorg. Mater. USSR*, 1970, vol. 6, pp. 1693–95.
23. S.F. Marenkin, S.I. Maksimova, B. Khuseinov, and V.Y. Shevchenko: *Inorg. Mater. USSR*, 1970, vol. 14, pp. 295–98.
24. V.B. Lazarev, N.P. Luzhnaya, S.F. Marenkin, V.Y. Shevchenko, and S.F. Chistov: *Zh. Neorg. Khim.*, 1972, vol. 17, pp. 1620–22.
25. K.L. Komarek, A. Mikula, and E. Hayer: *Ber. Bunsenges. Phys. Chem.*, 1976, vol. 80, pp. 765–70.
26. Z. Pruchnik: *Mater. Sci.*, 1977, vol. 3, pp. 121–25.
27. K. Yamaguchi, A. Mikula, K. Komarek, and K. Itagaki: *Z. Metall.*, 1991, vol. 82, pp. 591–98.
28. K. Friedrich and A. Leroux: *Metallurgie*, 1906, vol. 3, pp. 477–79.
29. W. Heike: *Z. Anorg. Chem.*, 1921, vol. 118, pp. 264–68.
30. V. Lazarev, S.F. Marenkin, S.I. Maksimova, B. Hkuseinov, and V.Y. Shevchenko: *Izv. Akad. Nauk SSSR Neorg. Mater.*, 1979, vol. 15, pp. 586–87.
31. V.B. Lazarev, V.N. Guskov, and J.H. Greenberg: *Mater. Res. Bull.*, 1981, vol. 16, pp. 1113–20.
32. A. Hrubý: *Czech. J. Phys. B*, 1976, vol. 26, pp. 593–98.
33. W. Spring: *Ber. Deut. Chem. Ges.*, 1883, vol. 16, pp. 324–26.
34. A. Granger: *Compt. Rend.*, 1904, vol. 138, pp. 574–75.
35. W. Trzebiatowski, F. Krolicld, and W. Zdanowicz: *Bull. Acad. Pol. Sci. Ser. Sci. Chim.*, 1968, vol. 16, pp. 343–46.
36. A. Pietraszko and K. Lukaszewicz: *Phys. Status Solidi (a)*, 1973, vol. 18, pp. 723–30.
37. G.B. Bokii, G.I. Goncharenko, G.G. Dvoryankina, V.I. Kovalev, and V.Y. Shevchenko: *Dokl. Akad. Nauk SSSR*, 1970, vol. 195, pp. 603–06.
38. Y.A. Ugai and T.A. Zyubina: *Izv. Akad. Nauk SSSR Neorg. Mater.*, 1965, vol. 1, pp. 860–67.
39. Y.A. Ugai, T.A. Zyubina, and K.B. Aleinikova: *Izv. Akad. Nauk SSSR Neorg. Mater.*, 1968, vol. 4, pp. 17–21.
40. H. Okamoto: *JPE*, 1992, vol. 13, pp. 147–54.
41. A.E. Vol and I.K. Kagan, *Cadmium Arsenic (Cd-As)*, National Bureau of Standards and National Science Foundation, Washington, DC, 1986, pp. 136–57.
42. A. Hrubý and L. Štourač: *Mater. Res. Bull.*, 1971, vol. 6, pp. 247–50.
43. H.J. Naake and C.S. Belcher: *J. Appl. Phys.*, 1964, vol. 35, pp. 3064–65.
44. G.A. Castellion and L.C. Beegle: *J. Phys. Chem. Solids*, 1965, vol. 26, pp. 766–73.
45. K. Masumoto, S. Isomura, and W. Gotô: *J. Jpn. Inst. Met.*, 1967, vol. 31, pp. 594–600.
46. V.M. Glazov and M. Kasymova: *Dokl. Akad. Nauk SSSR*, 1968, vol. 183, pp. 141–43.
47. S.E.R. Hiscocks: *J. Mater. Sci.*, 1969, vol. 4, pp. 773–78.
48. G.D. Nipan, V.B. Lazarev, and Y.K. Grinberg: *Russ. J. Inorg. Chem*, 1982, vol. 27, pp. 1008–010.
49. A.S. Jordan: *J. Electrochem. Soc. Solid State Sci.*, 1971, vol. 118, pp. 1362–65.
50. J.B. Clark and C.W.F.T. Pistorius: *High Temp. High Press.*, 1973, vol. 5, pp. 319–26.
51. S.F. Marenkin, A.Y. Vol'fkovich, S.G. Mikhailov, and V.V. Astakhov: *Inorg. Mater.*, 2003, vol. 39, pp. 911–15.
52. V.P. Sanygin, S.G. Mikhailov, K.K. Palkina, A.V. Steblevskii, A.M. Kvardakov, and S.F. Marenkin: *Inorg. Mater.*, 2005, vol. 41, pp. 3–6.
53. H. Okamoto: *J. Phase Equilib.*, 1992, vol. 13, pp. 155–61.
54. A. Descamps, *C. R. Hebd. Seances Acad. Sci.*, 1878, vol. 86, pp. 1065–66.
55. W. Zdanowicz, F. Krolicki, and P. Plenkiewicz: *Acta Phys. Pol. A*, 1973, vol. 4, p. 447.
56. G.A. Silvey: *J. Appl. Phys.*, 1958, vol. 29, pp. 226–27.
57. A. Jayaraman, T.R. Anantharaman, and J.W. Klement: *J. Phys. Chem. Solids*, 1966, vol. 27, pp. 1605–09.
58. J.H. Greenberg, V.N. Guskov, and V.B. Lazarev: *J. Chem. Thermodyn.*, 1985, vol. 17, pp. 739–46.
59. Z. Munir: *Science*, 1974, vol. 6, pp. 73–79.
60. O. Kubaschewski, E.L. Evans, and C.B. Alcock: *Metallurgical Thermochemistry*, 4th ed. Pergamon Press, Oxford, 1967.
61. E. Scheil and A. Kalkuhl: *Z. Metall.*, 1961, vol. 52, p. 557.
62. Y.M. Ivanov and Y.A. Kaller: *Chalcogenides of Zinc, Cadmium and Mercury*, Metallurgiya, Moscow, 1973.
63. A. Mikula and K. Komarek: *Int. J. Mater. Res.*, 1990, vol. 81, pp. 209–13.
64. S.A. Shchukarev, M.P. Morozova, and M.M. Bortnikova: *Z. Obshchel Khim.*, 1958, vol. 28, pp. 3289–92.
65. N.N. Sirota and E.M. Sklyarenko, *Russian Metallurgy (Metally)*, 1968, vol. 5, pp. 159–61.
66. A.F. Demidenko, G.N. Danilenko, V.E. Danilenko, V.B. Lazarev, V. Ya Shevchenko, S.F. Marenkin, and S.E. Koslov: *Izvestiya Akademii Nauk SSSR Neorg. Mater.*, 1977, vol. 13, pp. 214–16.
67. A.N. Nesmeyanov, B.Z. Iofa, A.A. Strelnikov, and V.G. Fursov: *Z. Fizichesko. Khim.*, 1956, vol. 30, pp. 1250–57.
68. V.J. Lyons and V.J. Silvestri: *J. Phys. Chem.*, 1960, vol. 64, pp. 266–69.
69. J.B. Westmore, K.H. Mann, and A.W. Tickher: *J. Appl. Chem.*, 1964, vol. 68, pp. 606–12.
70. E.S. Kalevich, S.P. Marenkin, V.F. Ponomarev, and V.Y. Shevchenko: *Izv. Akad. Nauk SSSR Neorg. Mater.*, 1978, vol. 14, pp. 1593–95.
71. G.N. Danilenko, V.E. Danilenko, M.K. Karapet'yants, V.B. Lazarev, S.F. Marenkin, and V. Shevchenko: *Izv. Akad. Nauk SSSR Neorg. Mater.*, 1977, vol. 13, pp. 1736–38.
72. S.F. Marenkin, V.B. Lazarev, V.Y. Shievchenko, and K.A. Sokolovsky: *J. Cryst. Growth*, 1980, vol. 50, pp. 761–63.

73. G. Natta and L. Passerini: *Gas. Chim. Ital.*, 1928, vol. 58, pp. 541–50.
74. S.M. Ariya, M.P. Morozova, T. Huan, and E. Volf: *Zh. Obshch. Khim.*, 1957, vol. 27, pp. 293–95.
75. V.E. Gorbunov, K.S. Gavrichev, G.A. Totrova, V.N. Guskov, J.H. Greenberg, and V.B. Lazarev: *Zh. Fiz. Khim.*, 1987, vol. 61, pp. 328–29.
76. R.C. Schoonmaker and K.J. Lemmerman: *J. Chem. Eng. Data*, 1972, vol. 17, pp. 139–43.
77. J.O. Andersson, T. Helander, L. Höglund, P. Shi, and B. Sundman: *Calphad*, 2002, vol. 26, pp. 273–312.
78. W. Zdanowicz, W. Trzebiatowski, and K. Lukaszewicz: *Bull. Acad. Pol. Sci. Sér. Sci. Chim.*, 1964, vol. 12, pp. 169–77.
79. L. Żdanowicz and W. Żdanowicz: *Physica Status Solidi (b)*, 1964, vol. 6, pp. 227–34.
80. S.F. Marenkin, I.S. Kovaleva, M. Saidullaeva, and V.P. Sanygin: *Izv. Akad. Nauk SSSR, Neorg. Mater.*, 1983, vol. 19, pp. 837–38.
81. J.A. Ugai, T.A. Zubina, and E.A. Malygin: *Neorg. Mater.*, 1966, vol. 17, pp. 876–80.
82. N.N. Sirota and É.M. Smolyarenko: *Chemical Bonds in Solids*, Springer, Boston, 1972.
83. A.T. Dinsdale: *Calphad*, 1991, vol. 15, pp. 317–425.
84. D.R. Stull and H. Prophet: *JANAF Thermochemical Tables*, U.S. Department of Commerce, Washington, DC, 1985.
85. S.A. Degterov, A.D. Pelton, and J.D. L'Ecuyer: *J. Phase Equilib.*, 1997, vol. 18, pp. 357–68.
86. O. Redlich and A.T. Kister: *Ind. Eng. Chem.*, 1948, vol. 40, pp. 345–48.
87. A.D. Pelton: *Calphad*, 2001, vol. 25, pp. 319–28.
88. M.N. Ali, Q. Gibson, S. Jeon, B.B. Zhou, A. Yazdani, and R.J.R.J. Cava: *Inorg. Chem.*, 2014, vol. 53, pp. 4062–67.
89. D. Koumoulis, R.E. Taylor, J. McCormick, Y.N. Ertas, L. Pan, X. Che, K.L. Wang, and L.S. Bouchard: *J. Chem. Phys.*, 2017, vol. 147, p. 084706.
90. L.M. Rogers, R.M. Jenkins, and A.J. Crocker: *J. Phys. D Appl. Phys.*, 1971, vol. 4, pp. 793–809.
91. H. Lu, X. Zhang, and S. Jia: *Sci. Rep.*, 2017, vol. 7, pp. 1–10.
92. G.F. Volodina, V.S. Zakhvalinskii, and V.K. Kravtsov: *Crystallogr. Rep.*, 2013, vol. 58, pp. 563–67.
93. S.F. Marenkin, V.A. Morozova, O.G. Koshelev, and G. Biskupski: *Physica Status Solidi (b)*, 1998, vol. 210, pp. 569–73.
94. V.A. Morozova, S.F. Marenkin, S.G. Mikhailov, and O.G. KosheleV: *Inorg. Mater.*, 2005, vol. 41, pp. 1039–42.
95. S.F. Marenkin, V.A. Morozova, and O.G. Koshelev: *Inorg. Mater.*, 2010, vol. 46, pp. 1001–06.
96. V.A. Morozova, S.F. Marenkin, O.G. Koshelev, D.V. Chernoguzov, S.G. Mikhailov, and A.V. Molchanov: *Inorg. Mater.*, 2007, vol. 43, pp. 215–20.
97. The Open Quantum Materials Database, https://oqmd.org/, accessed 22 December 2022.
98. The Materials Project, https://materialsproject.org/, accessed 26 December 2022.
99. A. Kubaschewski and C.B. Alcock: *Tables of Metallurgical Thermochemistry*, Elsevier Technology Books, London, 1979.
100. Thermal Constants of Materials (in Russian), Akad. Nauk SSSR, *Inst. Vys. Temp. Moscow*, 1972, vol. 6.
101. Z.A. Munir, G.B. Street, and N.F. Winters: *J. Chem. Phys.*, 1971, vol. 55, pp. 4520–27.
102. D.D. Wagman, W.H. Evans, V.B. Parker, R.H. Schumm, L. Halow, S.M. Bailey, L. Kenneth, and R. Nuttal: *J. Phys. Chem. Ref. Data*, 1982, vol. 11, pp. 37–38.
103. I. Barin: *Thermochemical Data of Pure Substances*, 3rd ed. VCH Verlag GmbH, Weinheim, 1995.
104. V.J. Lyons: *Phys. Chem.*, 1959, vol. 63, pp. 1142–44.
105. H. Hosono, K. Tanabe, E. Takayama-Muromachi, H. Kageyama, S. Yamanaka, H. Kumakura, M. Nohara, H. Hiramatsu, and S. Fujitsu, *Sci. Technol. Adv. Mater.*, 2015, vol. 16, p. 033503.
106. R. Pöttgen and D. Johrendt: *Intermetallics: Synthesis, Structure, Function*, 2nd ed. De Gruyter, Berlin, 2019.
107. N. Katayama, K. Kudo, S. Onari, T. Mizukami, K. Sugawara, Y. Sugiyama, Y. Kitahama, K. Iba, K. Fujimura, N. Nishimoto, M. Nohara, and H. Sawa, *J. Phys. Soc. Jpn.*, 2013, vol. 82, p. 123702.
108. W. Freyland: *Physics of Non-Tetrahedrally Bonded Elements and Binary Compounds I/Physik Der Nicht-tetraedrisch Gebundenen Elemente und Binären Verbindungen I*, Springer, Berlin, 1983.
109. N.I. Kopylov, Y.D. Kaminsky, and G.A. Tolstikov, Arsenic (in Russian), Siberia, 2004.
110. N.A. Gokcen: *Bull. Alloy Phase Diagrams*, 1989, vol. 10, pp. 11–22.
111. C.C. Herrick and R.C. Feber: *J. Phys. Chem.*, 1968, vol. 72, pp. 1102–110.